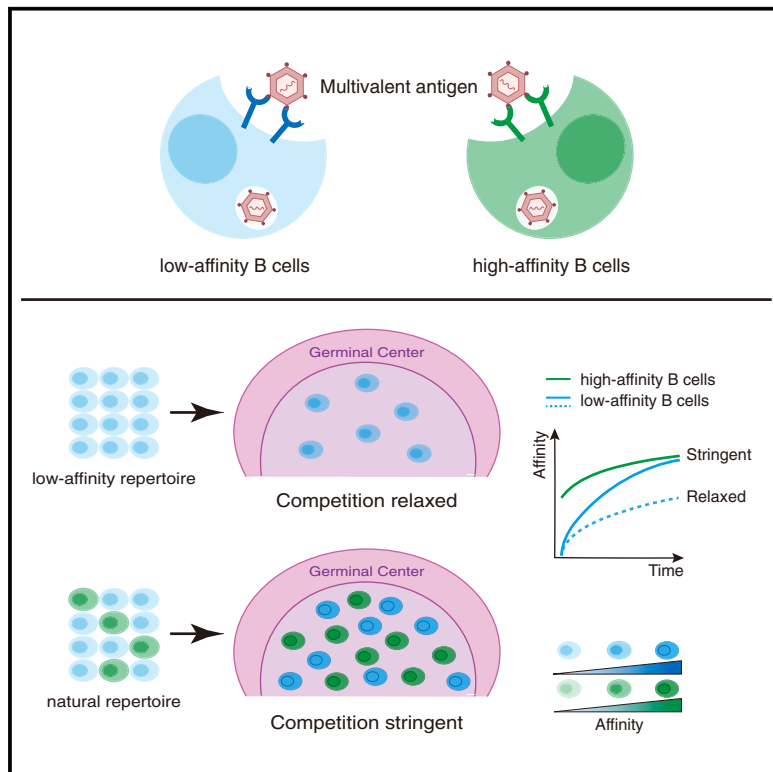


Competition propels, rather than limits, the success of low-affinity B cells in the germinal center response

Graphical abstract



Authors

Runhan Li, Keyan Bao, Can Liu,
Xuejing Ma, Zhaolin Hua, Ping Zhu,
Baidong Hou

Correspondence

zlhua@moon.ibp.ac.cn (Z.H.),
zhup@ibp.ac.cn (P.Z.),
baidong_hou@ibp.ac.cn (B.H.)

In brief

Competition from high-affinity B cells has long been viewed as an obstacle for low-affinity B cells entering GC responses. However, Li et al. demonstrate, using a multivalent virus-like particle antigen, that low-affinity B cells not only survive but also benefit from competition, with the affinity maturation process accelerated.

Highlights

- Low-affinity B cells participate in the GC response alongside high-affinity B cells
- Low-affinity and high-affinity B cells compete for the same epitope
- High-affinity B cell competition accelerates affinity maturation in low-affinity B cells
- Avidity may compensate for multivalent antigen binding in low-affinity B cells



Article

Competition propels, rather than limits, the success of low-affinity B cells in the germinal center response

Runhan Li,^{1,4} Keyan Bao,^{2,4} Can Liu,³ Xuejing Ma,^{1,3} Zhaolin Hua,^{1,3,*} Ping Zhu,^{1,2,3,*} and Baidong Hou^{1,3,5,*}

¹State Key Laboratory of Epigenetic Regulation and Intervention, Institute of Biophysics, Chinese Academy of Sciences, Beijing 100101, China

²National Laboratory of Biomacromolecules, Institute of Biophysics, Chinese Academy of Sciences, Beijing 100101, China

³University of Chinese Academy of Sciences, Beijing 100049, China

⁴These authors contributed equally

⁵Lead contact

*Correspondence: zlhua@moon.ibp.ac.cn (Z.H.), zhup@ibp.ac.cn (P.Z.), baidong_hou@ibp.ac.cn (B.H.)

<https://doi.org/10.1016/j.celrep.2025.115334>

SUMMARY

The germinal center (GC) sets an environment where antigen-specific B cells are compelled to continuously increase their affinity to compete for the antigen and obtain Tfh help for survival and propagation. Previous studies indicated that low-affinity B cells are disadvantaged in the presence of high-affinity ones, suggesting that competition may lead to the elimination of low-affinity B cells and their descendants. However, using a multivalent virus-mimicking antigen, our study demonstrates that low-affinity B cells not only successfully participate in GC responses alongside high-affinity B cells but also undergo accelerated affinity maturation under the more stringent competition. Furthermore, our cryo-electron-microscopy-based structural analysis reveals that both low-affinity and high-affinity B cells compete for the same antigenic epitope. Although the applicability of this idealized GC competition to true pathogen-induced responses remains uncertain, this change in perspective on the role of competition in low-affinity B cell evolution provides valuable insights for vaccine development.

INTRODUCTION

The germinal center (GC) response plays a crucial role in generating effective anti-viral responses.^{1–3} Within the GC, a competitive process akin to Darwinian selection occurs among B cells, driving antibody affinity maturation.^{1,4} Previous studies have demonstrated that the competition for entry into the GC can restrict the participation of low-affinity B cells in the GC response.^{5,6} However, broadly neutralizing antibodies (bnAbs) often originate from B cells with initially low affinity,^{7–10} suggesting that low-affinity B cells are not always outcompeted by their high-affinity counterparts.

While the permissiveness of low-affinity GC B cells has been observed,^{11,12} their long-term fate and competitive potential remain poorly understood. Despite their apparent ability to participate in the GC response, the mechanisms that govern their survival and selection over time are not fully elucidated. In addition, the phenomenon of immunodominance, where certain epitopes elicit a stronger immune response than others, is often attributed to competition between high-affinity and low-affinity B cells, with high-affinity B cells suppressing those recognizing subdominant epitopes^{10,13,14}—a view that has shaped many vaccine development strategies.^{15,16}

Here, we present evidence challenging the long-held view that competition between high-affinity and low-affinity B cells puts

the latter at a disadvantage. Contrary to this belief, our findings demonstrate that not only can low-affinity B cells survive the competition within the GC but they can also undergo accelerated affinity maturation under the pressure of competition. This sheds new light on the dynamics of the GC response and offers insights into the mechanisms underlying the development of effective immune responses.

RESULTS

Low-affinity B cells participate in the GC response in the presence of high-affinity B cells

We previously used Q β -VLP as a model antigen due to its ability to induce B cell Toll-like receptor (TLR) signaling, which is crucial for several aspects of anti-viral responses,^{17–19} including induction of T-independent antibody responses, GC responses, and the initiation of Tfh development independent of dendritic cells (DCs).²⁰ Our study focuses on antigen-specific B cells, which are directly relevant to immune protection, rather than bystander responses.

To isolate antigen-specific B cells, Q β -VLP was labeled with AF647, and anti-AF647-conjugated magnetic beads were used to enrich Q β -binding B cells while depleting non-binding cells (Figure S1A). To validate the efficiency of this procedure, splenocytes from naive mice were depleted or mock depleted



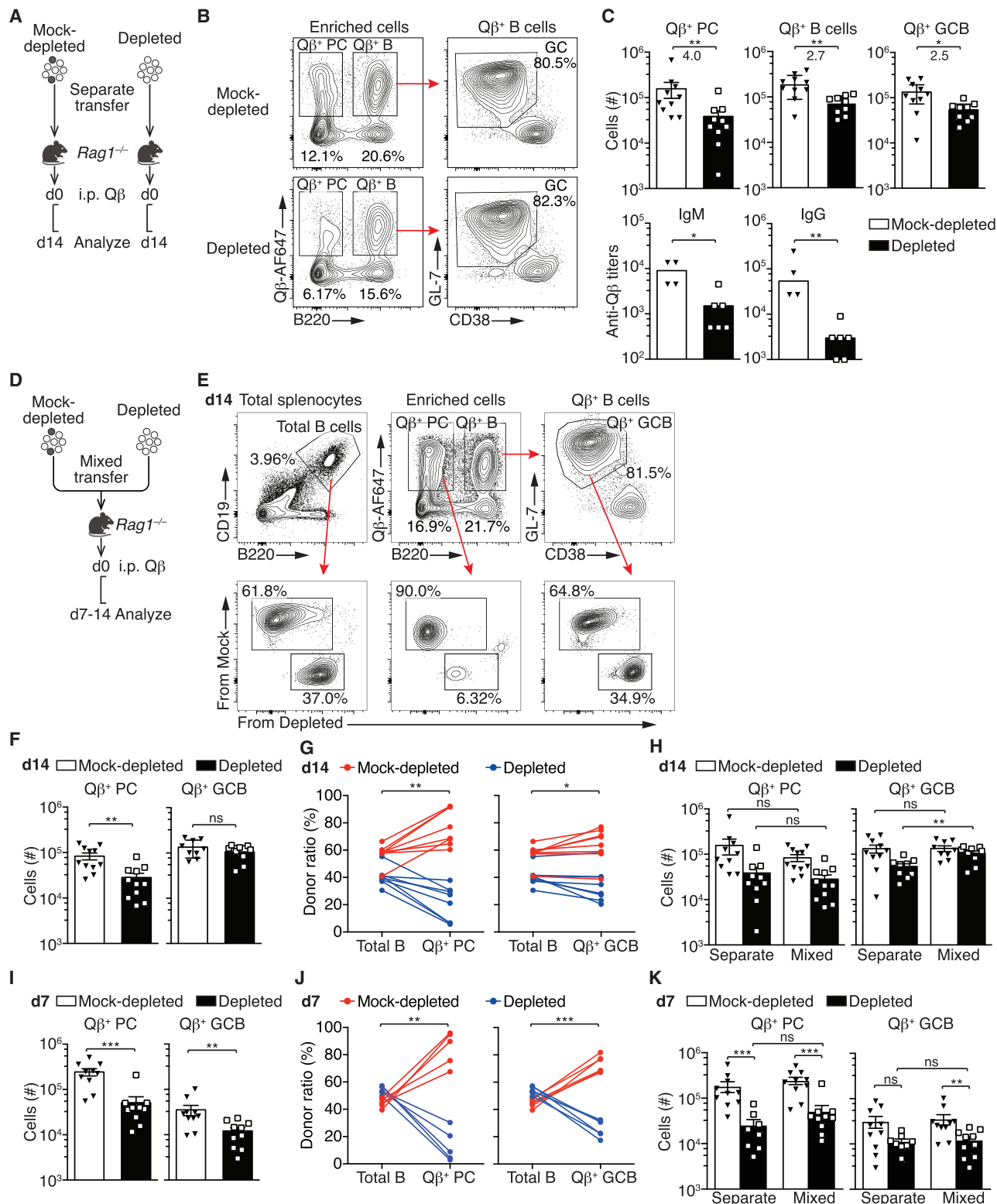


Figure 1. Low-affinity B cells participate in GC response in the presence of high-affinity B cells

(A) Experimental setup for (B and C). Splenocytes from C57BL/6 mice, depleted or mock depleted of Q β -AF647 $^{+}$ cells (Figure S1A), were transferred into Rag $^{1-/-}$ mice. Mice were then immunized and analyzed.

(legend continued on next page)

of Q β -binding cells and transferred to *Rag1*^{-/-} mice, which were then immunized and analyzed (Figure 1A). Mice receiving Q β -depleted cells showed significantly lower levels of anti-Q β antibodies and Q β ⁺ plasma cells (PCs) for both IgM and switched Ig isotypes compared with those receiving mock-depleted cells (Figures 1B, 1C, and S1B–S1D), confirming our expectations. However, these mice retained a robust Q β ⁺ GC response, with GC B cell numbers being less affected than PC numbers by Q β ⁺ cell depletion (Figures 1B and 1C). This finding suggests that the Q β -depleted fraction still contained B cells capable of responding to Q β -VLP.

Previous studies showed that B cells with antigen-binding affinities below detection limits can undergo affinity maturation through somatic hypermutation (SHM) and acquire binding capabilities.^{21–23} To distinguish between inefficient depletion and SHM-mediated affinity increase in Q β ⁻ B cells, we used splenocytes from *Aicda*^{-/-} mice, which lack activation-induced cytidine deaminase (AID), the key enzyme for SHM.²⁴ *Rag1*^{-/-} mice were transferred with either mock-depleted or Q β -depleted *Aicda*^{-/-} splenocytes, followed by immunization (Figure S1E). Mock-depleted *Aicda*^{-/-} splenocytes generated similar numbers of Q β ⁺ PCs and GC B cells as mock-depleted wild-type (WT) cells (Figures S1F and S1G), suggesting that AID deficiency does not significantly affect the proliferation or differentiation of these cells. In contrast, Q β -depleted *Aicda*^{-/-} splenocytes produced significantly fewer Q β ⁺ PCs and GC B cells compared with either mock-depleted *Aicda*^{-/-} cells or Q β -depleted WT cells (Figures S1F and S1G), indicating that AID is necessary for the Q β ⁻ B cells in the depleted fraction to enhance their binding capabilities. These results suggest that the Q β -depleted cell fraction contained B cells capable of responding to Q β -VLP, likely with low initial affinity, which was subsequently improved through SHM.

Previous studies have shown that low-affinity B cells for a hapten antigen are outcompeted by high-affinity B cells during a GC response.^{5,6} If the Q β -depleted cell fraction contained low-affinity B cells toward Q β -VLP, one might expect that they would be excluded from the GC response or exhibit reduced efficiency in the presence of higher-affinity Q β -binding B cells. To test this hypothesis, we mixed Q β -depleted and mock-depleted splenocytes from congenic mice carrying either the CD45.1 or CD45.2 allele at a 1:1 ratio before transferring them to *Rag1*^{-/-} mice (Figure 1D). Under these competitive conditions, although the Q β -depleted cells generated fewer PCs, they generated nearly equivalent numbers of Q β ⁺ GC B cells compared with the mock-depleted cells (Figures 1E–1G). This finding suggests that, despite the presence of higher-affinity B cells, the low-affin-

ity B cells can actively participate in and contribute to the GC response. The presence of Q β -depleted cells within the same anatomical GC structures as the mock-depleted cells was confirmed by immunohistochemistry (Figures S2A and S2B).

It is noteworthy that the mock-depleted cell fraction exhibited a greater capability to generate PCs compared with the Q β -depleted fraction (Figure 1F), consistent with the presence of higher-affinity B cells for Q β -VLP. At day (d)7 after immunization, mock-depleted cells produced significantly more PCs and GC B cells than Q β -depleted cells (Figures 1I–1K and S1H–S1J), indicating an initial advantage for high-affinity Q β -binding B cells over low-affinity cells. Additionally, the mock-depleted fraction generated more Q β ⁺ memory B cells alongside PCs (Figures S1K and S1L), likely due to greater expansion within the original Q β ⁺ cell populations.

Together, these results suggest that, while the low-affinity B cells initially lag behind in terms of the Q β -induced GC B cell number, they are capable of catching up with the high-affinity cells over time. Indeed, the Q β -depleted cell fraction generated more Q β ⁺ GC B cells under mixed transfer than separate transfer conditions (Figure 1H), indicating that low-affinity B cells not only survive but also thrive in competitive environments.

Low-affinity B cells bind to the same epitopes as high-affinity B cells

Previous studies have hypothesized that competition among GC B cells toward complex antigens, which contain more antigen epitopes than hapten antigens, might be less stringent.^{11,12} Therefore, we wondered whether low-affinity B cells bind different epitopes on Q β -VLP than high-affinity cells. To address this question, antibodies from single-sorted Q β ⁺ GC B cells were obtained from normally immunized WT mice (natural condition) or *Rag1*^{-/-} mice transferred with Q β -depleted cells (low-affinity-derived condition) (Figure 2A; Table S1). Q β -Ab complexes were prepared, and their cryo-electron microscopy (cryo-EM) structures determined (Video S1). Consistent with previously resolved high-resolution cryo-EM structure,^{25,26} Q β -VLP in the complexes exhibited a T=3 icosahedral symmetry, while the capsid protein (CP) presented three conformations (A, B, and C), enabling it to fit into three distinct local environments. The capsid comprises 90 CP dimers, with AB dimers radiating from the 5-fold axis and CC dimers filling the 2-fold axis (Figure S3A). The CP dimer contained a loop region between two N-terminal β -strands (β_A - β_B loop) that extended outward from the capsid (Figure 2B).

Q β -specific antibodies from natural and low-affinity GC B cells showed diverse VH and V κ use (Figure S3B). We determined the structures of a total of 24 Q β -Ab complexes (Figures S3C–S3F).

(B) Representative flow cytometry of Q β ⁺ PCs and GC B cells from Q β -AF647 enriched splenocytes.

(C) Quantification of Q β ⁺ cell numbers and anti-Q β antibodies, with fold differences between conditions indicated.

(D) Experimental setup for (E–G and I–J). Splenocytes from CD45.1⁺ and CD45.2⁺ mice, depleted or mock-depleted, were mixed 1:1 and transferred into *Rag1*^{-/-} mice. Mice were analyzed at d7 or d14 after immunization.

(E) Representative flow cytometry of donor contributions to total B cells, Q β ⁺ PC, and GC B cells at d14.

(F and G) Quantification of cell numbers and donor contributions to Q β ⁺ PC or GC B cells at d14.

(H) Combined comparison of Q β ⁺ cell numbers from (C) (separate) and (F) (mixed).

(I and J) Similar analysis as (F and G) at d7.

(K) Similar quantifications as (H) at d7.

Bars represent means, dots represent individual mice. Paired Student's t test (G, J) and Mann-Whitney test (C, F, H, I, and K) with p values (* <0.05 , ** <0.01 , *** <0.001).

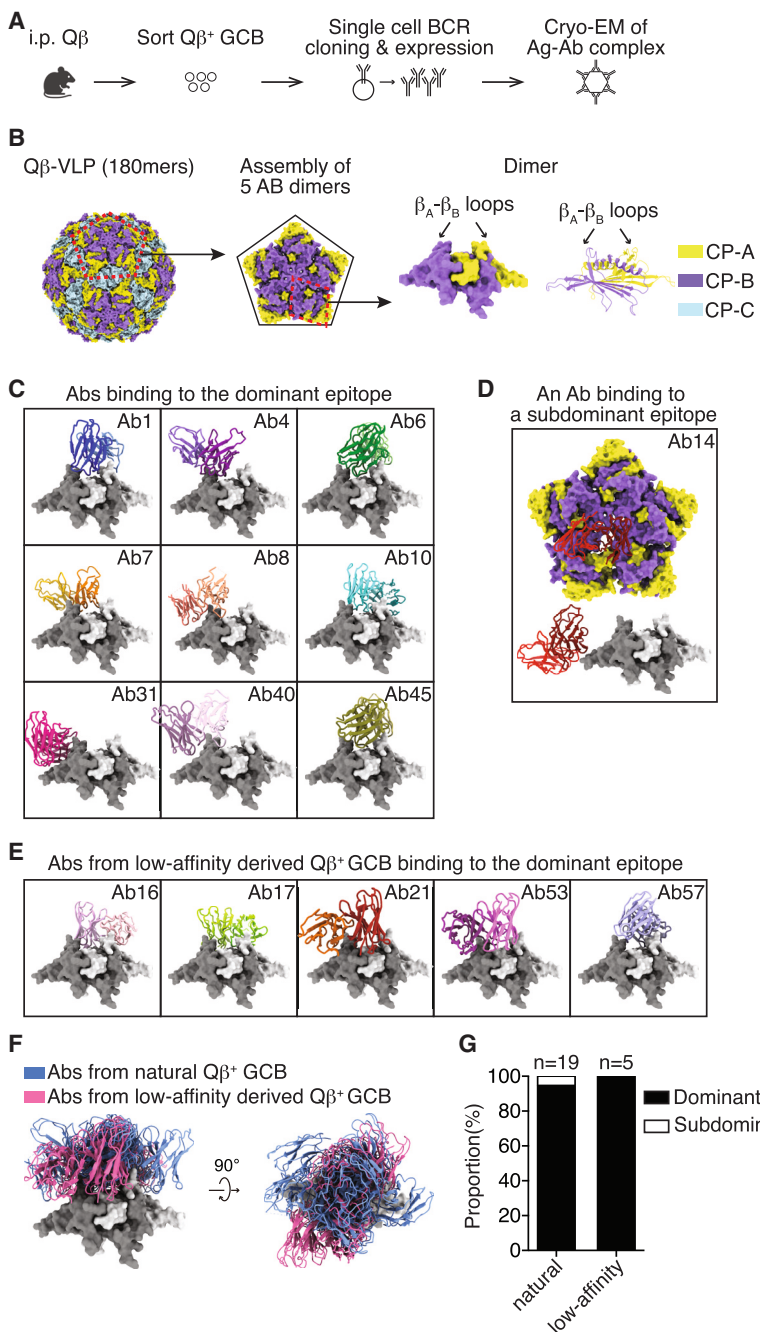


Figure 2. Low-affinity B cells bind to the same epitopes as high affinity B cells

(A) Experimental setup for structural analysis of Ag-Ab complexes via cryo-EM.

(B) Q β -VLP assembly from 180 CP subunits with distinct conformations (CP-A, -B, -C). β_A - β_B loop regions within an AB dimer are indicated.

(C–E) Fab structures (cartoon mode) from natural (C and D) or low-affinity-derived (E) Q β^+ GC B cells in complex with AB dimers (surface mode).

(F) Alignment of Fab-AB-dimer complexes from (C) and (E) shows overlap of antibodies derived from natural and low-affinity Q β^+ GC B cells. (Ab31, binding to the side of the dominant epitope, is excluded).

(G) Proportions of antibodies binding dominant or subdominant epitopes.

presenting one site and each CC dimer binding two antibodies simultaneously (Figure S3E).

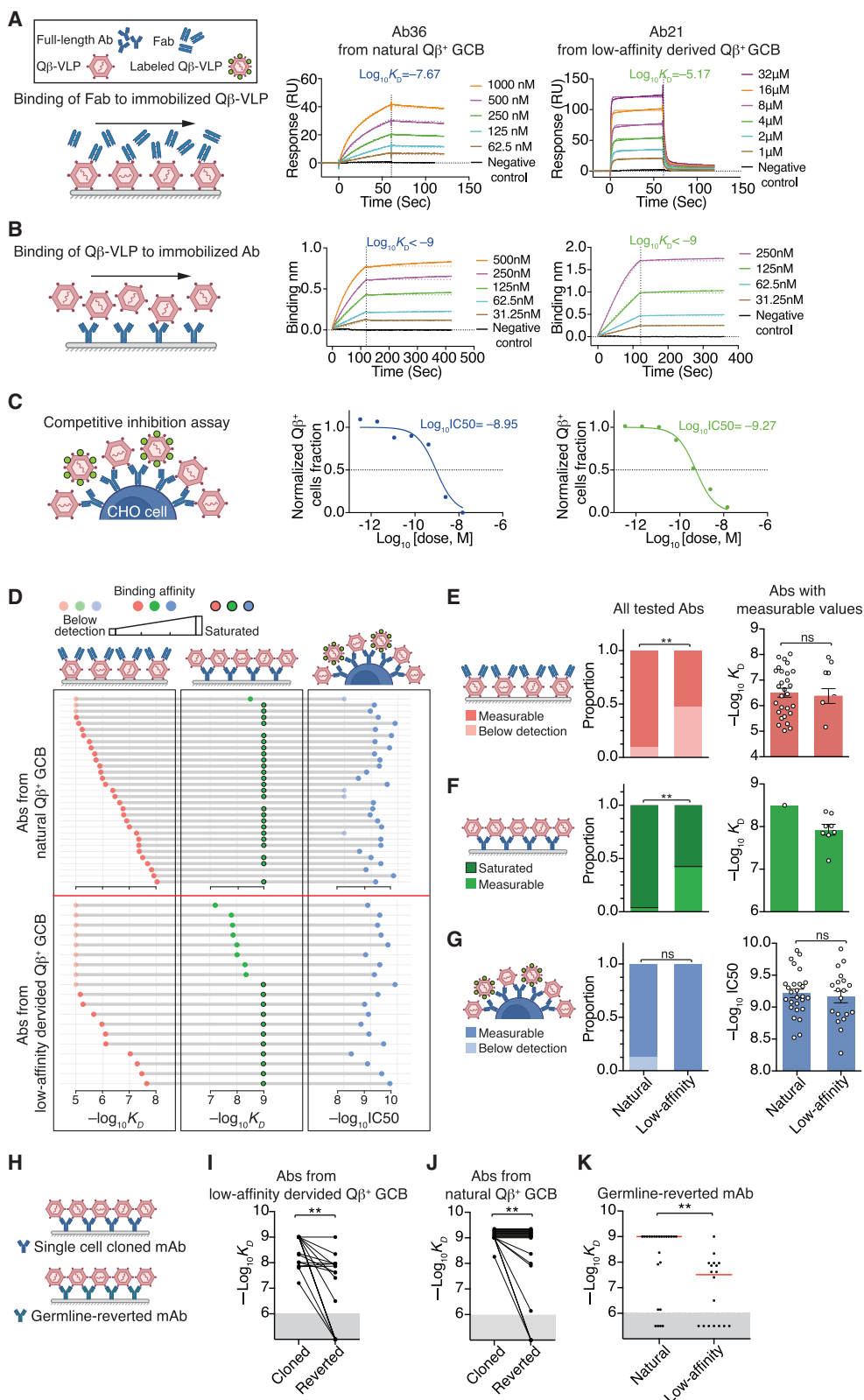
Together, we found that 23 of the 24 antibodies bound to the β_A - β_B loop region of the Q β -VLP. This suggests that Q β -VLP possesses a single dominant epitope located at the β_A - β_B loop (Figure 2C). Out of all the 24 resolved antibody structures, only one antibody was found to bind outside of the β_A - β_B loop region (Figures 2D and S3D). This epitope is located at the 5-fold axis, and only 12 binding sites are available on the Q β -VLP for this antibody. Thus, this epitope represents a subdominant epitope of the Q β -VLP.

We then compared the binding sites of antibodies derived from natural and low-affinity GC B cells. Among the nine antibodies from natural Q β^+ GC B cells that bind to the β_A - β_B loop, eight approach the loop region from above, while Ab31 approaches it from the side (Figures 2C, S3D, and S3E). All five antibodies from low-affinity-derived GC B cells bind to the β_A - β_B loop and approach it from above (Figures 2E and S3F). Furthermore, the binding patterns of the low-affinity B cell-derived antibodies completely overlap with those derived from natural Q β^+ GC B cells (Figure 2F). No antibodies from low-affinity-derived GC B cells were found to bind to the subdominant epitope (Figure 2G). These findings suggest that low-affinity B cells directly compete with high-affinity B cells for the same epitope.

Avidity compensates for antigen binding by low-affinity B cells

The observation that low-affinity B cells exhibit equal competitiveness as high-affinity B cells raises questions about how this

Among them, 15 were obtained at near-atom resolution, allowing us to build atomic models (Figures 2C–2E; Table S2). We also mapped the epitopes for the remaining nine antibodies, although the resolutions were relatively low (Figures S3D and S3E). Most antibodies exhibit either 60 or 90 binding sites on Q β -VLP, indicating their predominantly binding to AB dimers or both AB and CC dimers (Figures S3D–S3F). Antibodies exhibiting 90 binding sites access the two symmetric epitopes on the dimer with steric clash, resulting in only one antibody bound to the dimer. We also identified an antibody that binds to 120 sites, with each AB dimer



(legend on next page)

aligns with their reduced antigen acquisition and lower chance of interacting with cognate Tfh cells, which are crucial for GC B cell differentiation.^{27–29}

To directly quantify differences in antigen binding capacity, we measured both the strict-term affinity—direct binding affinity between the antibody Fab fragment and its epitope (Figure 3A), and the functional affinity, which accounts for avidity effects from antibody bivalence and the multivalency of Q β -VLP (Figures 3B and 3C). Two methods (Figures 3A and 3B) relied on binding kinetics, while the third (Figure 3C) used competitive inhibition.

First, we compared the strict-term affinity of antibodies from natural and low-affinity-derived Q β ⁺ GC B cells (Figures 3D and 3E; Table S3). Antibodies from natural Q β ⁺ GC B cells showed a wide range of affinities (from 10⁻⁵ to 10⁻⁸ M), while a significantly greater proportion of antibodies from low-affinity-derived Q β ⁺ GC B cells were below detection limits (Figures 3D and 3E), consistent with their low-affinity origin. Among antibodies with measurable binding kinetics, no significant differences were observed in K_{on} , K_{off} , or K_D between the two groups (Figures 3E and S4A), suggesting overlapping affinity ranges.

While this result confirms that low-affinity-derived GC B cells indeed exhibit lower affinity at the population level, it does not fully explain their competitiveness within the GC response. The ability of low-affinity B cells to effectively compete with high-affinity B cells remains unanswered. To investigate whether the binding capacity of low-affinity B cells could be compensated by avidity, we used the second method, measuring the functional affinity between Q β -VLP and full-length antibodies immobilized on a solid surface (Figure 3B). Using this method, antibodies undetectable in the first method now exhibited measurable Q β -VLP binding (Figures 3D and 3F). Additionally, a substantial fraction of antibodies displayed very slow off rates, causing saturation in affinity measurements. Although a significantly greater proportion of antibodies from natural GC B cells exhibited saturated K_{off} and K_D values, indicating a greater affinity at the population level, antibodies from low-affinity-derived GC B cells nonetheless displayed equivalent or slightly higher K_{on} compared with the natural group (Figure S4B). Overall, these results indicate that avidity may compensate for the binding of low-affinity B cells to Q β -VLP.

To further evaluate whether multivalent binding could account for the competence of low-affinity B cells at the cellular level, we expressed these antibodies on CHO cells and conducted the

competitive inhibition assay (Figure 3C). In this assay, cells were divided into multiple fractions, and varying concentrations of unlabeled Q β -VLP were added to generate concentration-dependent inhibitory curves. The half-maximal inhibitory concentration (IC_{50}) was used to indicate affinity (Figures S4C and S4D). Using this approach, the IC_{50} values for antibodies from low-affinity-derived B cells showed no significant difference compared with those from natural Q β ⁺ GC B cells (Figure 3D and 3G), suggesting that low-affinity B cells may acquire comparable amounts of antigen *in vivo*. It also implies that avidity, resulting from multiple antibody-antigen interactions, may mitigate the disadvantage of low-affinity B cells.

To confirm that low-affinity B cells gain affinity through SHM, we tested germline-reverted antibodies for Q β -VLP binding using ELISA (Figure S4E) and kinetic assays (Figure 3H). Germline-reverted antibodies exhibited a significant decrease in antigen binding, supporting that low-affinity B cells undergo SHM to increase affinity to Q β -VLP (Figures 3I and S4F). Since natural Q β ⁺ GC B cell antibodies also gained affinity via SHM (Figure 3J), the affinities of germline-reverted antibodies from the two groups were compared. While there is some overlap, germline-reverted antibodies from low-affinity-derived B cells exhibit significantly lower affinities than those from natural Q β ⁺ GC B cells (Figure 3K), further confirming that what we defined as the low-affinity B cells indeed show lower binding kinetics at the population level.

Since the low-affinity B cells participated the GC response successfully, we were curious as to whether the low-affinity B cells represent polyreactive or autoreactive B cells. To test this hypothesis, we assessed the binding of Q β ⁺ GC B cell derived antibodies to double-stranded DNA, insulin, and lipopolysaccharide. A small fraction of these antibodies exhibited weak binding to these antigens (Figures S5A and S5B). However, there was no significant difference of the polyreactivity between the natural and low-affinity-derived antibodies. In addition, we also examined the polyreactivity of the corresponding germline-reverted antibodies. For the low-affinity B cell derived antibodies, there seemed a trend of increased polyreactivity upon germline reversion, but it did not reach statistical significance (Figures S5C and S5D).

Together, these results support the notion that multivalency and avidity effects could contribute to the competitiveness of low-affinity B cells in the GC response, enabling them to effectively compete with high-affinity B cells despite their lower affinity at the individual B cell receptor level.

Figure 3. Avidity compensates for antigen binding by low-affinity B cells

(A–C) Schematics and representative data for antibody affinity assays. (A) Binding kinetics of Fab to immobilized Q β -VLP measured by surface plasmon resonance. (B) Binding kinetics of Q β -VLP to immobilized full-length Abs by bio-layer interferometry. (C) Binding of Q β -VLP to membrane-bound Abs by competitive inhibition assay.

(D) Affinity results for antibodies from natural (d14 or d28 after immunization) and low-affinity (d28) derived Q β ⁺ GC B cells. Each row shows data for a single antibody; light-colored dots indicate below detection and black-bordered dots for saturation.

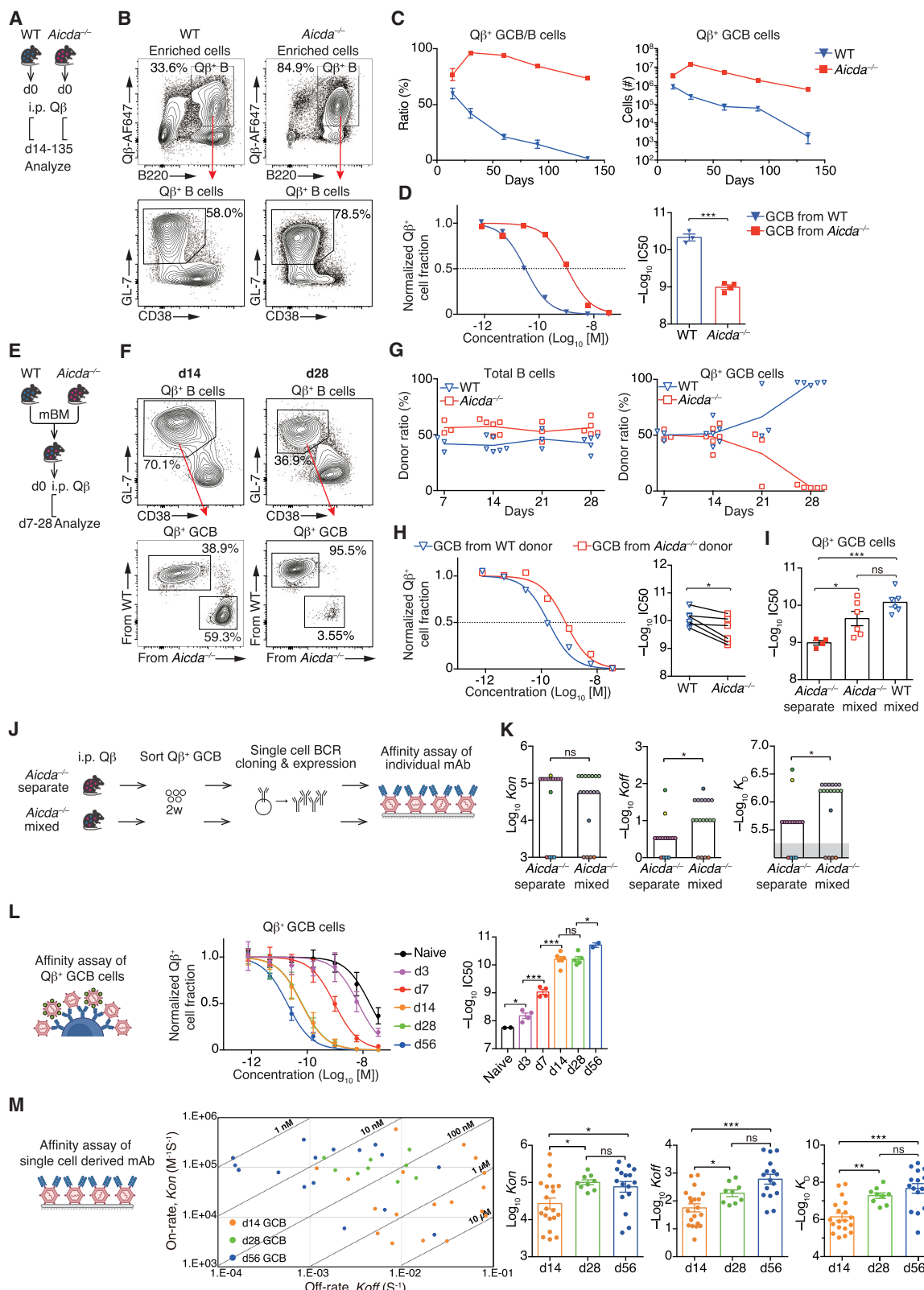
(E–G) Summary of data in (D). Left bar graphs show proportions of antibodies below detection limits, within measurable range, or saturated (chi-square test). Right bar graphs display values for antibodies within measurable range.

(H) Germline-reverted antibodies (reverted) were generated for mAbs cloned (cloned) from single cells, and measured for affinities as in (B).

(I and J) Affinities of antibodies from low-affinity-derived (I) or natural (J) Q β ⁺ GC B cells vs. their germline-reverted counterparts.

(K) Comparison of germline-reverted antibody affinities from (I) and (J). Data points below $-\log_{10}K_D = 6$ (gray region) are below detection; those at $-\log_{10}K_D = 9$ are saturated.

Mann-Whitney test (E–G, K) and paired Student's t test (I, J) with p values (ns, non-significant; **p < 0.01).



(legend on next page)

Competition accelerates the affinity maturation of low-affinity B cells

Given that the avidity could compensate for the antigen binding by the low-affinity B cells, we wondered whether GC competition becomes less stringent and more permissive. To test this hypothesis, we first examined GC B cells from *Aicda*^{-/-} mice, which lack the ability to increase antibody affinity through SHM (Figure 4A). *Aicda*^{-/-} mice displayed a robust Q β ⁺ GC response, with a higher number and longer persistence of Q β ⁺ GC B cells compared with WT mice (Figures 4B and 4C), likely due to reduced apoptosis in *Aicda*^{-/-} GC B cells.³⁰ Given the abundance of Q β ⁺ GC B cells in these mice, we measured their Q β -binding affinity at the population level using the competitive inhibition assay (Figure 4D). *Aicda*^{-/-} GC B cells collected 2 weeks after immunization exhibited significantly lower affinity than their WT counterparts (Figure 4D), confirming that SHM enhances affinity in WT GC B cells.

We then investigated whether *Aicda*^{-/-} Q β ⁺ GC B cells could participate in the GC response alongside WT GC B cells by generating mixed bone marrow (BM) chimeric mice containing *Aicda*^{-/-} and WT BM cells, followed by immunization (Figure 4E). *Aicda*^{-/-} Q β ⁺ GC B cells coexisted with WT GC B cells without notable disadvantage for up to 2–3 weeks after immunization (Figures 4F and 4G). Surprisingly, the affinity of *Aicda*^{-/-} GC B cells in the mixed BM mice was significantly higher than those in the absence of WT chimerism, almost approaching the affinity of WT Q β ⁺ GC B cells (Figures 4H and 4I). Since *Aicda*^{-/-} GC B cells cannot increase affinity through SHM, the observed increase likely reflects the selection of higher-affinity B cells already present in their native repertoire. To test this hypothesis, single Q β ⁺ GC B cells from *Aicda*^{-/-} mice, either in the absence or presence of WT chimerism, were sorted, and their derived antibodies were assessed for affinity to Q β -VLP (Figure 4J). Antibodies from *Aicda*^{-/-} Q β ⁺ GC B cells under both conditions displayed strong oligoclonality, with multiple clones sharing identical Ig sequences. Although the affinity ranges in both conditions were similar, the dominant clones from the mixed chimerism condition exhibited significantly higher affinity than those from separate *Aicda*^{-/-} mice (Figure 4K), confirming that *Aicda*^{-/-} cells with higher affinity were preferentially selected under competitive pressure. Together, these results suggest that vigorous compe-

tion exists among Q β -specific GC B cells, resulting in strong selection for the high-affinity B cells.

To evaluate the persistence of *Aicda*^{-/-} GC B cells under competition from WT cells, BM chimeric mice were analyzed at later time points. By 3–4 weeks after immunization, *Aicda*^{-/-} Q β ⁺ GC B cells decreased sharply and nearly vanished (Figures 4F and 4G). In contrast, *Aicda*^{-/-} cells remained markedly abundant in the Q β ⁻ GC B cell subset (Figures S6A–S6C). These findings indicate that the decline of *Aicda*^{-/-} Q β ⁺ GC B cells in the presence of WT counterparts was not due to intrinsic defects, such as class-switch issues or altered apoptosis rates. Instead, it likely reflects the limited maximum affinity that *Aicda*^{-/-} Q β ⁺ GC B cells can achieve. This suggests that the permissiveness for low-affinity B cells in response to this multivalent antigen remains very limited.

To further understand the dynamics of affinity maturation in GC B cells under physiological conditions, we immunized WT mice with Q β -VLP and measured the change in affinity of Q β ⁺ GC B cells over 2 months (Figure 4L). During the first 2 weeks, the affinity of GC B cells, indicated by the IC₅₀ of Q β binding measured by the competitive inhibition assay, increased and reached the same level as PCs at d14 (Figures 4L and S6D). From 2 weeks onward, the affinity showed limited increase and seemed to reach a plateau (Figure 4L). Meanwhile, Q β ⁺ memory B cells gradually caught up to the affinity of GC B cells by 4–5 months (Figure S6E).

Although these results align with the established understanding that higher affinity B cells differentiate into PCs and the lower affinity B cells become memory B cells during GC B cell differentiation,³¹ they alone do not explain the elimination of *Aicda*^{-/-} GC B cells in the BM chimeric mice after 3–4 weeks of immunization. To determine if the affinity of Q β ⁺ GC B cells truly reaches a plateau, antibodies cloned from single GC B cells isolated between 2 weeks and 2 months after immunization in WT mice were analyzed for their affinity to Q β -VLP using the binding kinetic assay (Figure 4M). The results showed that while affinity at the cellular level reached a near plateau by 2 weeks (Figure 4L), affinity at the Fab level continued to increase up to 8 weeks (Figure 4M). This increase was paralleled with the rising mutation rates in the antibodies (Figure S6F). These results suggest that, while the GC environment may be permissive for individual GC

Figure 4. Competition promotes selection of high-affinity B cells in *Aicda*^{-/-} mice

- (A) Experimental setup for (B–D). WT and *Aicda*^{-/-} mice were immunized and analyzed.
- (B) Representative flow cytometry of Q β ⁺ GC B cells on d14 after immunization.
- (C) Quantification of Q β ⁺ GC B cell ratios and numbers over 135 days.
- (D) Affinity of Q β ⁺ GC B cells measured by competitive inhibition assay on d14 after immunization. Each point represents two pooled mice.
- (E) Experimental setup for (F–I). Mixed BM (mBM) chimeric mice generated from WT (CD45.1⁺) and *Aicda*^{-/-} (CD45.2⁺) were immunized and analyzed 7–28 days after immunization.
- (F and G) Donor contributions to Q β ⁺ GC B cells over time.
- (H) Affinity of Q β ⁺ GC B cells from chimeric mice at d14 after immunization, with donors from the same mice connected.
- (I) Affinity of *Aicda*^{-/-} Q β ⁺ GC B cells in separate (A) vs. mixed (E) conditions, with WT values included for reference. (I) Shares the same data with (D) and (H).
- (J) Single-clone affinity analysis setup for *Aicda*^{-/-} Q β ⁺ GC B cells.
- (K) Summary of binding kinetics (*K*_{on}, *K*_{off}, and *K*_D = *K*_{off}/*K*_{on}) for *Aicda*^{-/-} antibodies in separate vs. mixed conditions, with bars as medians. Clones with identical sequences are shown in the same color. Gray shading indicates values below detection limits.
- (L and M) Progressive affinity maturation of Q β ⁺ GC B cells in WT mice at population (L) and clonal (M) levels. (L) Affinity at different time points was measured by competitive inhibition assay, with each dot representing data from two pooled mice. (M) Single-cell-derived mAbs were analyzed for *K*_{on}, *K*_{off}, and *K*_D (on an oblique scale). Data are summarized with bars as means and dots as individual data.

Paired t test (H), unpaired t test (L), and Mann-Whitney test (D, I, K, M) with *p* values (ns, non-significant; **p* < 0.05, ***p* < 0.01, ****p* < 0.001).

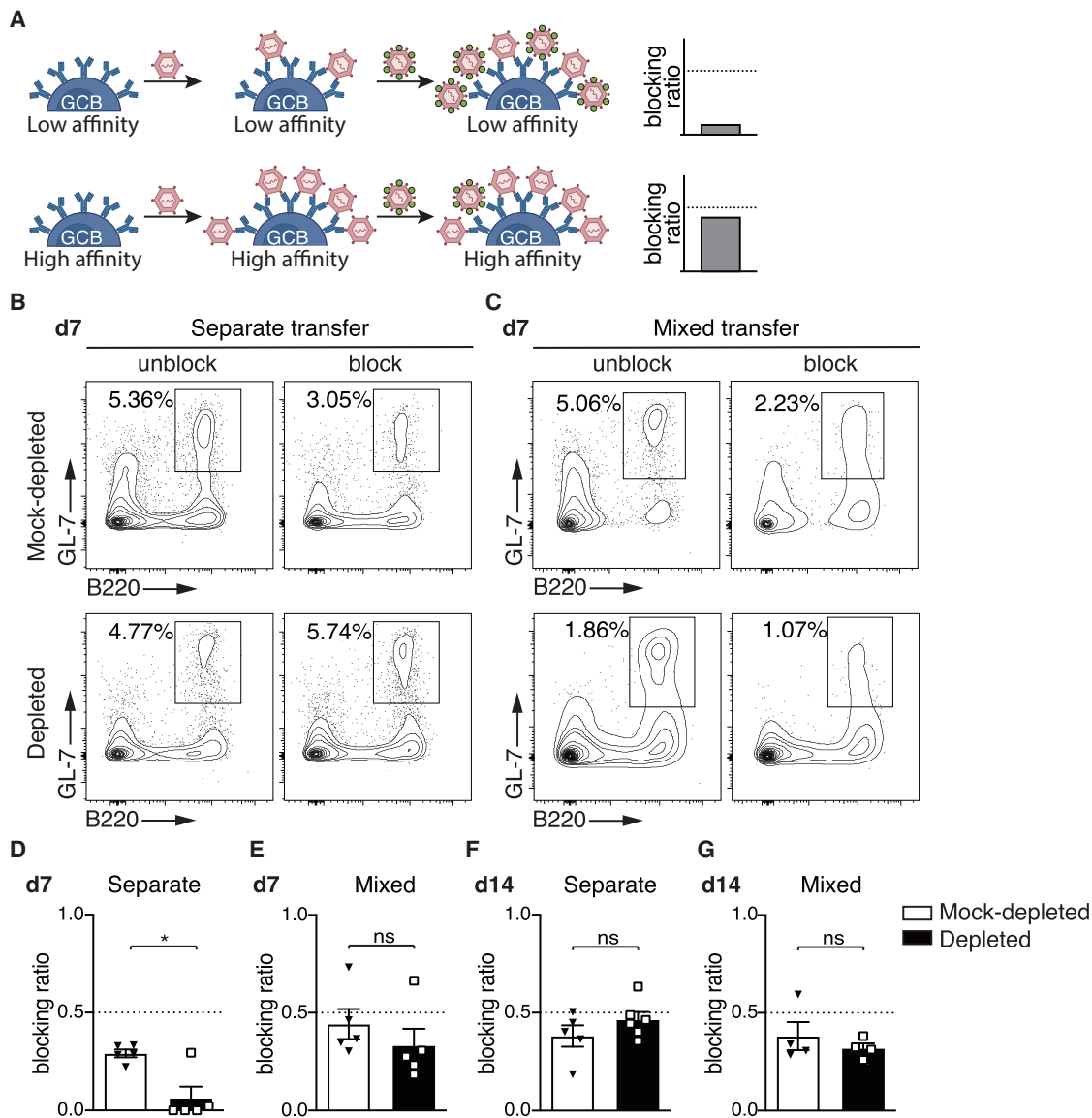


Figure 5. Competition accelerates affinity maturation in low-affinity B cells

(A) Schematic of modified competitive inhibition assay using blocking ratios as measurements. Lower-affinity B cells bind less unlabeled Q β -VLP, resulting in a lower blocking ratio. Unlabeled Q β -VLP concentrations were approximately 0.6 nM for d7 and approximately 0.06 nM for d14 samples.

(B and C) Representative blocking ratio assay data from adoptive transfer experiments on d7 after immunization. Q β -depleted or mock-depleted splenocytes were transferred separately (B) or mixed (C) into *Rag1* $^{-/-}$ mice, followed by immunization. Splenocytes from *Rag1* $^{-/-}$ mice were incubated with (block) or without (unblock) unlabeled Q β -VLP, followed by Q β -AF647 incubation. Q β -AF647 $^+$ cells were enriched using magnetic beads. Flow cytometry shows the percentage of GL-7 $^+$ B220 $^+$ GC B cells in the enriched fraction.

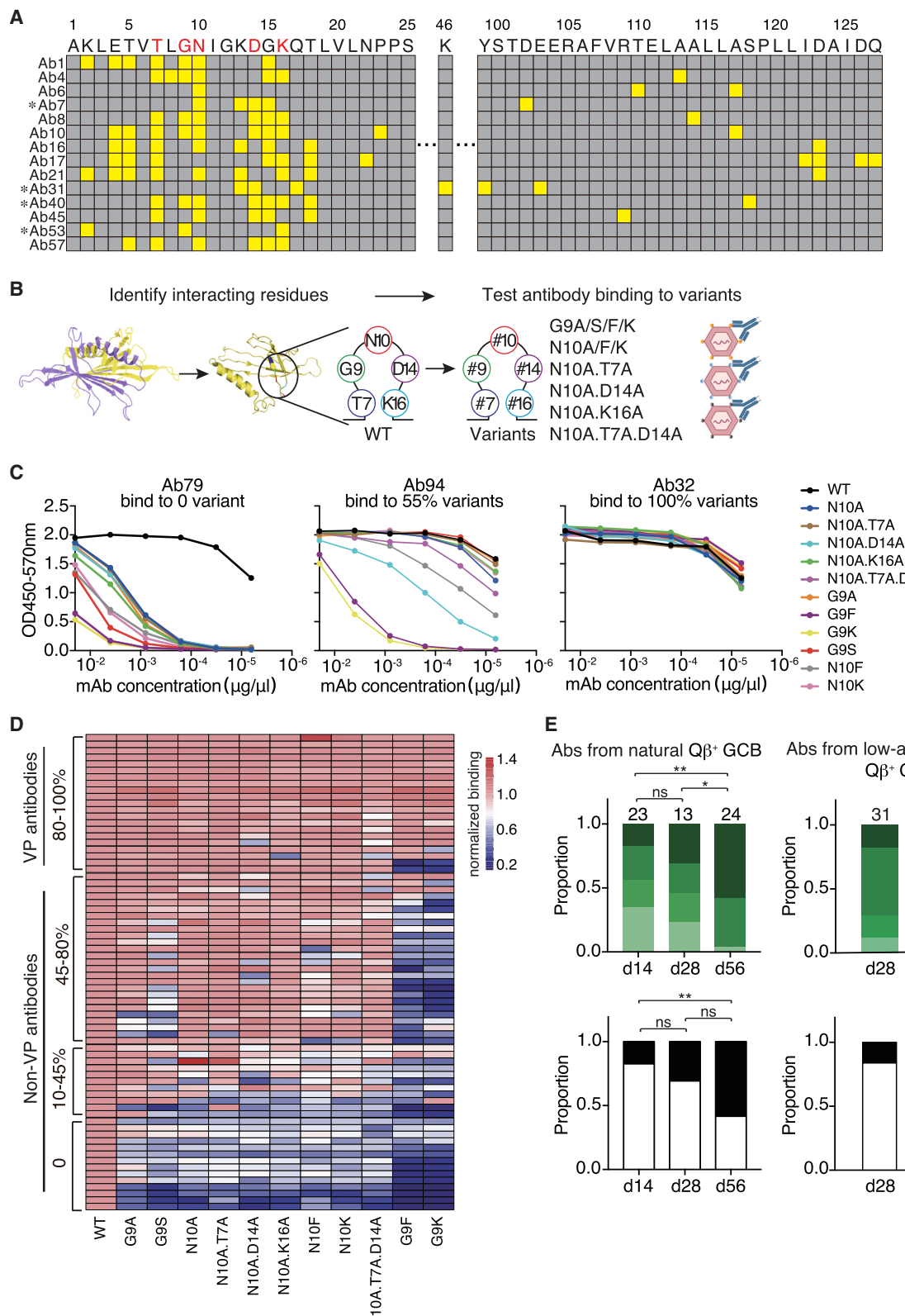
(D–G) Blocking ratios of Q β $^+$ GC B cells under indicated conditions.

Mann-Whitney test with p values (ns, non-significant; *p < 0.05).

B cells with lower affinity, competitive pressures within GCs persist, driving a continuous increase in overall affinity at the population level. This observation may also explain the rapid decline of *Aicda* $^{-/-}$ Q β $^+$ GC B cells in the mixed BM chimeric mice, as the affinity difference between WT and *Aicda* $^{-/-}$ GC B cells likely increases over time, eventually leading to the outcompetition of *Aicda* $^{-/-}$ GC B cells by the WT cells. Further study is needed to determine whether this continuous increase in affinity

is due to a mechanism of antibody feedback³² or direct competition among GC B cells.

To investigate the impact of competition on the affinity maturation of low-affinity B cells, we compared the process in the presence or absence of high-affinity B cells using the adoptive transfer experiments (Figure 5). Due to the scarcity of Q β $^+$ B cells in *Rag1* $^{-/-}$ mice with transferred cells, we modified the competitive inhibition assay. In this assay, splenocytes were incubated



(legend on next page)

with a fixed concentration of unlabeled Q β -VLP, followed by binding to AF647-labeled Q β -VLP (Figure 5A). The concentration of unlabeled Q β -VLP was set to approximately the IC₅₀ value measured for GC B cells from WT mice immunized over the same time course (Figure 4L) to maximize the likelihood of detecting potential affinity differences. The blocking ratio, which reflects relative affinity, was then compared, with a higher blocking ratio indicating higher affinity.

In separate adoptive transfer experiments, the Q β^+ GC B cells derived from Q β -depleted cells showed a lower blocking ratio at d7 after immunization compared with those from mock-depleted cells (Figures 5B and 5D), reflecting their lower affinities. However, under mixed transfer conditions, the Q β^+ GC B cells derived from the Q β -depleted fraction displayed an increased blocking ratio, reaching levels comparable to those from mock-depleted cells (Figures 5C and 5E). These results suggest that competition from high-affinity B cells accelerates the affinity maturation of low-affinity B cells. At d14 after immunization, there was no significant difference in the blocking ratio for Q β^+ GC B cells between Q β -depleted and mock-depleted conditions, in both separate and mixed transfer experiments (Figures 5F and 5G). This is likely due to the inability of this assay in distinguishing affinity differences as the affinity matures further, as previously demonstrated (Figures 3G and 4L).

Overall, these results indicate that competition plays a role in promoting the affinity maturation of low-affinity B cells in response to a multivalent antigen. In the presence of high-affinity B cells, the low-affinity B cells undergo affinity maturation at a faster rate, driven by competition within the GC environment, leading to the selection and improvement of lower-affinity B cells.

Low-affinity B cells contribute partly to variant-proof antibodies

If the sole purpose of GC competition is to increase the affinity of B cell receptors, one might question the physiological significance of facilitating the affinity maturation of low-affinity B cells when high-affinity B cells already possess an advantage. We wondered whether the low-affinity-derived GC B cells might exhibit increased resistance to antigen mutations, similar to the case of HIV bnAbs.^{9,33} To test this hypothesis, we introduced single or combined mutations at the β_A - β_B loop region, the dominant epitope of the Q β protein (Figures 6A, 6B, and S7A), and measured the binding capability of monoclonal antibodies to these variant forms Q β -VLP.

Most antibodies exhibited reduced binding to the Q β -VLP variants (Figures 6C and 6D; Table S4). The polyclonal antibodies from immunized mice also exhibited reduced binding to all the tested variants (Figure S7B). These results confirmed

that the β_A - β_B loop consists of the dominant immune epitope of the Q β -VLP. Intriguingly, a subset of antibodies show no significant decrease in binding to multiple variants compared with the original form of Q β -VLP (Figures 6C and 6D), a characteristic we define as variant proof (VP). Moreover, a greater proportion of antibodies derived from later stages of the GC response exhibited VP features, indicating an increased prevalence of VP antibodies over time (Figure 6E). A proportion of low-affinity-derived antibodies also displayed VP characteristics (Figure 6E), suggesting that low-affinity B cells can contribute to the generation of some VP antibodies. Notably, the emergence of VP antibodies occurred even without heterologous immunization, highlighting an underappreciated feature intrinsic to GC responses.

Theoretically, two mechanisms could underlie the observed VP binding. First, the binding site lies outside mutated regions, so the Ag-Ab interaction is unaffected by mutations. Indeed, antibody Ab14 (Figure 2D), which binds the subdominant epitope, exhibits VP characteristics. Second, antibodies bind to mutated regions but tolerate the mutations. Among the five VP antibodies for which Q β -Ab complex structures were resolved, four (Ab40, Ab7, Ab31, and Ab53) (Figures 2C and 2E) belong to this category. We wondered if VP antibodies evolve a larger interface area for interaction. However, no significant differences were observed in the CDR3 length, interface areas, or the number of interacting residues between VP and non-VP antibodies (Figure S7C). To gain further insights into the structural basis of VP binding, we determined the cryo-EM structures of two VP antibodies (Ab40 and Ab7) bound to both WT and variant forms of Q β -VLP (Figures 7 and S7D-S7F; Table S2). The overall orientation of VP antibodies remained unchanged when binding to variants compared with WT. In the case of single mutation variants, the β_A - β_B loop maintained its original orientation, while residues on the CDR3 loop of the antibody involved in the binding interface exhibited slight shifts to accommodate the binding (Figures 7A–7C). In the case of the triple mutation variant, the density of the N-terminal strand-loop region is missing (Figures 7D and 7E for Ab40; S7F for Ab7), suggesting a flexible feature in the binding between the antibodies and the triple mutation variant. These observations suggest that VP antibodies may be prone to catering to flexible geometry conformations, enabling them to effectively bind to variant antigens. Whether flexibility is a common feature for all VP antibodies that bind to the dominant epitope needs further study.

DISCUSSION

In this study, we demonstrated that low-affinity B cells can effectively participate in the Q β -VLP-induced GC response, even in the

Figure 6. Low-affinity B cells partly contribute to VP antibodies

- (A) Amino acids in Q β -VLP monomer that interact with antibodies are highlighted in yellow. VP antibodies (Ab7, 31, 40, and 53) are marked (*).
- (B) Diagram illustrating residues in the β_A - β_B loop being mutated to create Q β -VLP variants, which are further tested for antibody binding.
- (C) Representative ELISA data showing antibodies with varying binding capacities to Q β -VLP variants.
- (D) ELISA results quantified as area under the curve (AUC), normalized to the AUC for Q β ^{WT}, and visualized in a heatmap. area under the curve values of >0.9 indicate binding. Antibodies binding ≥ 9 variants (80–100%) are classified as VP, while others are non-VP.
- (E) Proportions of antibodies, derived from various sources at different time points, with different binding capacities to variants. Chi-square test was used, with p value shown (ns: non-significant, p* < 0.05, p** < 0.01).

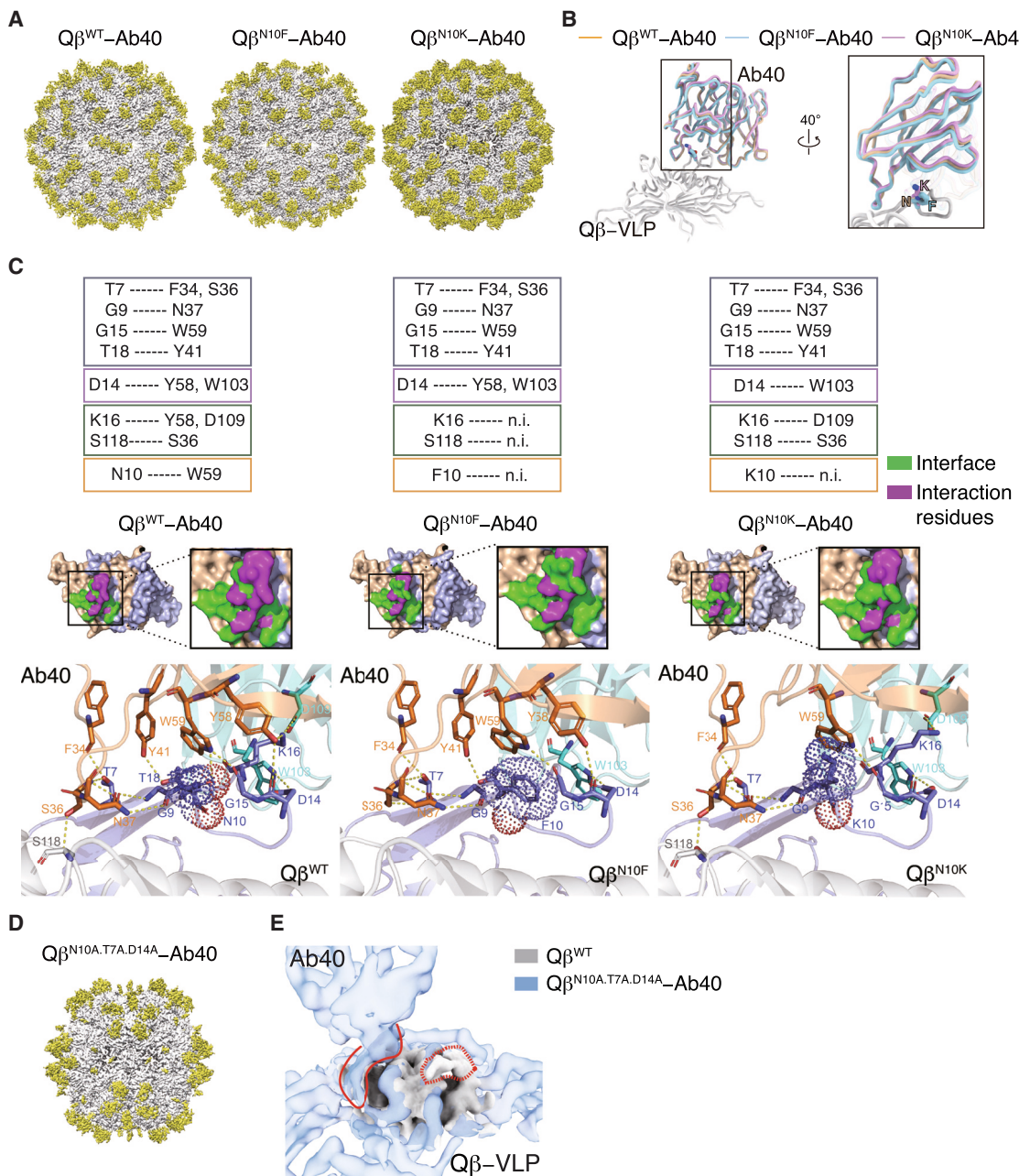


Figure 7. VP antibodies bind to $\text{Q}\beta$ -VLP with flexibility

(A) Global structures of VP antibody Ab40 in complex with $\text{Q}\beta^{\text{WT}}$, $\text{Q}\beta^{\text{N}10\text{F}}$, and $\text{Q}\beta^{\text{N}10\text{K}}$.

(B) Aligned Ab40 structures show subtle conformational changes for adaptation to variants binding.

(C) Interaction details of Ab40 with dimers in $\text{Q}\beta^{\text{WT}}$, $\text{Q}\beta^{\text{N}10\text{F}}$, and $\text{Q}\beta^{\text{N}10\text{K}}$. The interaction residues are listed and structurally depicted.

(D and E) Global (D) and zoom-in (E) structures of Ab40 in complex with $\text{Q}\beta^{\text{N}10\text{A.T}7\text{A.D}14\text{A}}$. (E) Cryo-EM densities of $\text{Q}\beta^{\text{N}10\text{A.T}7\text{A.D}14\text{A}}\text{-Ab40}$ complex (blue), aligned with densities of $\text{Q}\beta^{\text{WT}}$ (gray), reveal one $\beta_{\text{A}}\text{-}\beta_{\text{B}}$ loop with proper density (solid red line) and the other lacking density (dashed red line).

presence of high-affinity B cells, challenging the assumption that competition limits the involvement of low-affinity B cells.^{5,6,28,34} Our data suggest that GCs not only tolerate the presence of low-affinity B cells but also exert strong selection pressure on them, resulting in accelerated affinity maturation of low-affinity B cells.

Previous studies have demonstrated the capacity of GCs to accommodate B cells spanning a wide spectrum of affinities,^{11,12} a phenomenon also corroborated in our study (Figure 3). These observations have prompted the formulation of a permissive model aimed at elucidating the emergence of high-affinity anti-viral antibodies, including bnAbs, from low-affinity precursors.

While this model does not discount the notion of competition among GC B cells, it implies that competition may be less rigorous or more tolerant. However, our findings indicate that competition within our experimental settings is highly intense.

In a permissive scenario, one would expect a more equal representation of high-affinity and low-affinity cells in GCs at earlier rather than later time points post immunization. However, our data reveal a predominance of high-affinity B cells at earlier stages (d7) compared with later time points (d14) (Figures 1G and 1J), a trend incompatible with the permissive model. Furthermore, a reduction in the vigor of competition would theoretically result in reduced efficacy in affinity maturation. Indeed, it has been shown that when Tfh cells are less constrained, the affinity of GC B cells decrease rather than increase.²⁹ Our results further support this notion, as AID-deficient GC B cells exhibited lower affinity to Q β -VLP when alone, compared with when they faced competition from WT GC B cells (Figure 4I). Moreover, we also found that low-affinity B cells actually acquire affinity more rapidly when co-transferred with high-affinity counterparts (Figure 5), contradicting the expectations of the permissive model.

Thus, the success of low-affinity B cells in our experimental settings cannot be simply attributed to permissiveness. Rather, it is competition that exerts selection pressure and accelerates the evolutionary process of low-affinity B cells. This evolutionary process relies on the intrinsic ability of B cells to undergo SHM.

Then what factors could determine the success of low-affinity B cells in the face of competition? Original studies demonstrate the disadvantage of low-affinity B cells in hapten antigen-specific responses.^{5,6} It has been speculated that complex antigens, such as viral proteins, might create more permissive conditions for low-affinity B cells.¹¹ However, subsequent research shows that competition at different antigenic epitopes can also suppress the B cell response,³⁵ suggesting that antigen complexity alone does not determine the success of low-affinity B cells. In our study, the low-affinity B cells bind to the same epitope as the high-affinity cells (Figure 2), demonstrating that low-affinity B cells can succeed even under stringent competition.

One of the main features distinguishing Q β -VLP from previous model antigens is its multivalency. We found that avidity could partly compensate for the Q β -VLP binding by low-affinity B cells (Figure 3). It has also been shown that multimerization of an HIV-derived antigen strongly compensates for its weak immunogenicity.³⁴ However, there remains a clear difference in the initial binding capacities between low-affinity and high-affinity B cells. Whether the valency state of antigens is the major factor contributing to the success of low-affinity B cells needs further study.

Another important factor influencing the fate of low-affinity B cells may lie in the generation of Tfh cells. It has been observed that Tfh cells act as a limiting factor, creating a bottleneck for GC entry,^{28,29,35,36} which can lead to the elimination of low-affinity B cells. Our group previously demonstrated the existence of two independent antigen presentation pathways for initial CD4 T cell activation: the DC-dependent pathway for soluble protein immunization and the B cell-dependent pathway for TLR7 ligand-containing multivalent antigens like Q β -VLP.^{20,37} When B cells serve as primary antigen-presenting cells, Tfh limitation may be less prominent than when DCs are required. Since

both low-affinity and high-affinity B cells responding to Q β -VLP carry the same T cell antigens, they could share cognate T cell help, with high-affinity B cells potentially helping low-affinity ones by providing more Tfh cells. This might explain the result that low-affinity-derived GC B cells, in the presence of high-affinity B cells, even exceed in number compared with when high-affinity B cells are absent (Figure 1H). However, further investigation is needed to validate this hypothesis.

The GC response in anti-viral defenses holds significance in both affinity maturation and antibody diversification. Affinity maturation is crucial for eliminating viruses, while diversification addresses viral mutations.¹ Therefore, it is plausible that, although high-affinity B cells could produce strong antibodies, the inclusion of low-affinity B cells may generate a more diverse antibody repertoire, better suited for combating viral variants. Interestingly, GCs can produce B cells recognizing variant epitopes despite exposure to only WT virus,³⁸ highlighting the importance of antibody diversification during antiviral responses. Our findings demonstrate that low-affinity B cells contribute to VP antibodies against Q β -VLP, indicating a potential physiological importance for including low-affinity B cells in GC responses.

Our study also questions the relationship between immunodominance and the initial affinity of B cells recognizing different epitopes. When low-affinity B cells are outcompeted by high-affinity ones, affinity differences might drive immunodominance. However, when low-affinity B cells participate in GC responses, as shown in this study, other factors may outweigh initial affinity in determining the immunogenicity of an epitope. In fact, the only antibody (Ab14) binding the subdominant Q β -VLP epitope has higher affinity than antibodies targeting the dominant epitope at the same time points (Table S1). A similar phenomenon is seen with the HIV subdominant MPER epitope, where germline-reverted antibodies exhibit relatively high affinity than those for dominant epitopes.³⁹ This revised view of immunodominance and B cell competition has implications for vaccine strategies, especially for HIV and universal influenza vaccines.^{10,14,16,40} Although our study does not provide a direct solution to overcoming immunodominance, it suggests reducing competition may not always be beneficial.

Limitations of the study

This study leveraged Q β -VLP, a multivalent antigen with a single immunodominant epitope, to show from a manageable number of Ag-Ab complex structures that low-affinity B cells can compete with high-affinity ones for the same epitope. However, most pathogen antigens are more complex with multiple epitopes. How such complexity affects competition remains unclear.

Another limitation of Q β -VLP is its high multivalency. Viruses with lower antigen density may restrict low-affinity B cells' access to antigens, reducing their GC participation. Additionally, TLR signaling in B cells may influence outcomes. Q β -VLP-induced GC responses are impaired in the absence of B cell MyD88, likely affecting both high- and low-affinity cells, thus complicating the study of TLR function in low-affinity cells. Future studies with other multivalent antigens may clarify this.

Competition in this study occurred at the population level, allowing some low-affinity B cells to succeed. However, this does

not imply that all low-affinity B cells could achieve such success. A diverse repertoire of low-affinity B cells presumably increases these chances, as evidenced by the diverse VH and V_k usage elicited by Q β -VLP. Conversely, antigens activating limited repertoires may reduce opportunities for low-affinity cells to emerge.

In summary, Q β -VLP represents an idealized viral antigen and demonstrates the capacity to generate diverse antibodies from both high- and low-affinity precursors. To what extent true pathogens or vaccines can induce such immune responses requires further investigation.

RESOURCE AVAILABILITY

Lead contact

Requests for resources and reagents should be directed to and will be fulfilled by Baidong Hou (baidong_hou@ibp.ac.cn).

Materials availability

All unique reagents generated in this study are available from the [lead contact](#) with a completed Materials Transfer Agreement.

Data and code availability

- Cryo-EM information is listed in [Table S2](#) and the [key resources table](#).
- This paper does not report the original code.
- Any additional information required to reanalyze the data reported in this work paper is available from the [lead contact](#) upon request.

ACKNOWLEDGMENTS

This work was supported by the National Key Research and Development Program of China (2019YFA0508901, 2021YFC2300501, 2021YFA1300100, and 2018YFE0203300), CAS (XDB29050600 and XDB37010100), and NNSFC (81991495 and 32241029). *Aicda*^{-/-} mice were generated by the Transgenic Core of IBP. EM data were collected at the Center for Bio-imaging, IBP. We thank Yuanyuan Chen, Zhenwei Yang, and Bingxue Zhou for technical support on BLI and SPR.

AUTHOR CONTRIBUTIONS

R.L., K.B., and C.L. performed the experiments. X.M. assisted the experiments. P.Z., Z.H., and B.H. designed and supervised the study. Z.H. and B.H. wrote the manuscript.

DECLARATION OF INTERESTS

The authors declare no competing interests.

STAR★METHODS

Detailed methods are provided in the online version of this paper and include the following:

- [KEY RESOURCES TABLE](#)
- [EXPERIMENTAL MODEL AND STUDY PARTICIPANT DETAILS](#)
 - Experimental animals
 - Cell lines and culture conditions
- [METHOD DETAILS](#)
 - Expression and purification of Q β -VLP and variants
 - Immunization
 - Adoptive transfer
 - Labeling and enrichment of antigen-specific B cells
 - Flow cytometry
 - Single cell sorting and cDNA synthesis
 - Ig gene amplification
 - Expression and purification of antibodies and Fab fragments

- Enzyme-linked immunosorbent assay (ELISA)
- Measurement of binding kinetics by surface plasmon resonance (SPR)
- Measurement of binding kinetics by biolayer interferometry (BLI)
- Competitive inhibition assay
- Negative staining electron microscopy analysis
- Cryo-EM data collection, processing and structure building

● QUANTIFICATION AND STATISTICAL ANALYSIS

- Statistical analysis

SUPPLEMENTAL INFORMATION

Supplemental information can be found online at <https://doi.org/10.1016/j.celrep.2025.115334>.

Received: June 18, 2024

Revised: December 1, 2024

Accepted: January 29, 2025

Published: February 15, 2025

REFERENCES

1. Victora, G.D., and Nussenzweig, M.C. (2022). Germinal Centers. *Annu. Rev. Immunol.* **40**, 413–442. <https://doi.org/10.1146/annurev-immunol-120419-022408>.
2. Elsner, R.A., and Shlomchik, M.J. (2020). Germinal Center and Extrafollicular B Cell Responses in Vaccination, Immunity, and Autoimmunity. *Immunity* **53**, 1136–1150. <https://doi.org/10.1016/j.immuni.2020.11.006>.
3. Bachmann, M.F., Odermatt, B., Hengartner, H., and Zinkernagel, R.M. (1996). Induction of long-lived germinal centers associated with persisting antigen after viral infection. *J. Exp. Med.* **183**, 2259–2269. <https://doi.org/10.1084/jem.183.5.2259>.
4. Bannard, O., and Cyster, J.G. (2017). Germinal centers: programmed for affinity maturation and antibody diversification. *Curr. Opin. Immunol.* **45**, 21–30. <https://doi.org/10.1016/j.co.2016.12.004>.
5. Shih, T.A.Y., Meffre, E., Roederer, M., and Nussenzweig, M.C. (2002). Role of BCR affinity in T cell dependent antibody responses *in vivo*. *Nat. Immunol.* **3**, 570–575. <https://doi.org/10.1038/ni803>.
6. Dal Porto, J.M., Haberman, A.M., Kelsoe, G., and Shlomchik, M.J. (2002). Very low affinity B cells form germinal centers, become memory B cells, and participate in secondary immune responses when higher affinity competition is reduced. *J. Exp. Med.* **195**, 1215–1221. <https://doi.org/10.1084/jem.20011550>.
7. Scheid, J.F., Mouquet, H., Feldhahn, N., Seaman, M.S., Velinzon, K., Pietzsch, J., Ott, R.G., Anthony, R.M., Zebroski, H., Hurley, A., et al. (2009). Broad diversity of neutralizing antibodies isolated from memory B cells in HIV-infected individuals. *Nature* **458**, 636–640. <https://doi.org/10.1038/nature07930>.
8. Dosenovic, P., Kara, E.E., Pettersson, A.K., McGuire, A.T., Gray, M., Hartweger, H., Thientosapol, E.S., Stamatatos, L., and Nussenzweig, M.C. (2018). Anti-HIV-1 B cell responses are dependent on B cell precursor frequency and antigen-binding affinity. *Proc. Natl. Acad. Sci. USA* **115**, 4743–4748. <https://doi.org/10.1073/pnas.1803457115>.
9. Wu, X., Zhang, Z., Schramm, C.A., Joyce, M.G., Kwon, Y.D., Zhou, T., Sheng, Z., Zhang, B., O'Dell, S., McKee, K., et al. (2015). Maturation and Diversity of the VRC01-Antibody Lineage over 15 Years of Chronic HIV-1 Infection. *Cell* **161**, 470–485. <https://doi.org/10.1016/j.cell.2015.03.004>.
10. Havenar-Daughton, C., Lee, J.H., and Crotty, S. (2017). Tfh cells and HIV bnAbs, an immunodominance model of the HIV neutralizing antibody generation problem. *Immunol. Rev.* **275**, 49–61. <https://doi.org/10.1111/imr.12512>.
11. Kuraoka, M., Schmidt, A.G., Nojima, T., Feng, F., Watanabe, A., Kitamura, D., Harrison, S.C., Kepler, T.B., and Kelsoe, G. (2016). Complex Antigens

- Drive Permissive Clonal Selection in Germinal Centers. *Immunity* 44, 542–552. <https://doi.org/10.1016/j.jimmuni.2016.02.010>.
12. Tas, J.M.J., Mesin, L., Pasqual, G., Targ, S., Jacobsen, J.T., Mano, Y.M., Chen, C.S., Weill, J.C., Reynaud, C.A., Browne, E.P., et al. (2016). Visualizing antibody affinity maturation in germinal centers. *Science* 351, 1048–1054. <https://doi.org/10.1126/science.aad3439>.
 13. Abbott, R.K., and Crotty, S. (2020). Factors in B cell competition and immunodominance. *Immunol. Rev.* 296, 120–131. <https://doi.org/10.1111/imr.12861>.
 14. Victora, G.D., and Wilson, P.C. (2015). Germinal center selection and the antibody response to influenza. *Cell* 163, 545–548. <https://doi.org/10.1016/j.cell.2015.10.004>.
 15. Silva, M., Nguyen, T.H., Philbrook, P., Chu, M., Sears, O., Hatfield, S., Abbott, R.K., Kelsoe, G., and Sitkovsky, M.V. (2017). Targeted Elimination of Immunodominant B Cells Drives the Germinal Center Reaction toward Subdominant Epitopes. *Cell Rep.* 21, 3672–3680. <https://doi.org/10.1016/j.celrep.2017.12.014>.
 16. Burton, D.R. (2019). Advancing an HIV vaccine; advancing vaccinology. *Nat. Rev. Immunol.* 19, 77–78. <https://doi.org/10.1038/s41577-018-0103-6>.
 17. Hou, B., Saudan, P., Ott, G., Wheeler, M.L., Ji, M., Kuzmich, L., Lee, L.M., Coffman, R.L., Bachmann, M.F., and DeFranco, A.L. (2011). Selective utilization of Toll-like receptor and MyD88 signaling in B cells for enhancement of the antiviral germinal center response. *Immunity* 34, 375–384. <https://doi.org/10.1016/j.jimmuni.2011.01.011>.
 18. Liao, W., Hua, Z., Liu, C., Lin, L., Chen, R., and Hou, B. (2017). Characterization of T-Dependent and T-Independent B Cell Responses to a Virus-like Particle. *J. Immunol.* 198, 3846–3856. <https://doi.org/10.4049/jimmunol.1601852>.
 19. Tian, M., Hua, Z., Hong, S., Zhang, Z., Liu, C., Lin, L., Chen, J., Zhang, W., Zhou, X., Zhang, F., et al. (2018). B Cell-Intrinsic MyD88 Signaling Promotes Initial Cell Proliferation and Differentiation To Enhance the Germinal Center Response to a Virus-like Particle. *J. Immunol.* 200, 937–948. <https://doi.org/10.4049/jimmunol.1701067>.
 20. Hong, S., Zhang, Z., Liu, H., Tian, M., Zhu, X., Zhang, Z., Wang, W., Zhou, X., Zhang, F., Ge, Q., et al. (2018). B Cells Are the Dominant Antigen-Presenting Cells that Activate Naive CD4(+) T Cells upon Immunization with a Virus-Derived Nanoparticle Antigen. *Immunity* 49, 695–708.e4. <https://doi.org/10.1016/j.jimmuni.2018.08.012>.
 21. Dal Porto, J.M., Haberman, A.M., Shlomchik, M.J., and Kelsoe, G. (1998). Antigen drives very low affinity B cells to become plasmacytes and enter germinal centers. *J. Immunol.* 161, 5373–5381. <https://doi.org/10.4049/jimmunol.161.10.5373>.
 22. Di Niro, R., Lee, S.J., Vander Heiden, J.A., Elsner, R.A., Trivedi, N., Bannock, J.M., Gupta, N.T., Kleinstein, S.H., Vigneault, F., Gilbert, T.J., et al. (2015). Salmonella Infection Drives Promiscuous B Cell Activation Followed by Extrafollicular Affinity Maturation. *Immunity* 43, 120–131. <https://doi.org/10.1016/j.jimmuni.2015.06.013>.
 23. Silver, J., Zuo, T., Chaudhary, N., Kumari, R., Tong, P., Giguere, S., Granato, A., Donthula, R., Devreux, C., and Wesemann, D.R. (2018). Stochasticity enables BCR-independent germinal center initiation and antibody affinity maturation. *J. Exp. Med.* 215, 77–90. <https://doi.org/10.1084/jem.20171022>.
 24. Muramatsu, M., Kinoshita, K., Fagarasan, S., Yamada, S., Shinkai, Y., and Honjo, T. (2000). Class switch recombination and hypermutation require activation-induced cytidine deaminase (AID), a potential RNA editing enzyme. *Cell* 102, 553–563. [https://doi.org/10.1016/s0092-8674\(00\)00078-7](https://doi.org/10.1016/s0092-8674(00)00078-7).
 25. Cui, Z., Gorzelnik, K.V., Chang, J.Y., Langlais, C., Jakana, J., Young, R., and Zhang, J. (2017). Structures of Qbeta virions, virus-like particles, and the Qbeta-MurA complex reveal internal coat proteins and the mechanism of host lysis. *Proc. Natl. Acad. Sci. USA* 114, 11697–11702. <https://doi.org/10.1073/pnas.1707102114>.
 26. Golmohammadi, R., Fridborg, K., Bundule, M., Valegård, K., and Liljas, L. (1996). The crystal structure of bacteriophage Q beta at 3.5 Å resolution. *Structure* 4, 543–554. [https://doi.org/10.1016/s0969-2126\(96\)00060-3](https://doi.org/10.1016/s0969-2126(96)00060-3).
 27. Crotty, S. (2011). Follicular Helper CD4 T Cells (T-FH). *Annu. Rev. Immunol.* 29, 621–663. <https://doi.org/10.1146/annurev-immunol-031210-101400>.
 28. Schwickert, T.A., Victora, G.D., Fooksman, D.R., Kamphorst, A.O., Mugnier, M.R., Gitlin, A.D., Dustin, M.L., and Nussenzweig, M.C. (2011). A dynamic T cell-limited checkpoint regulates affinity-dependent B cell entry into the germinal center. *J. Exp. Med.* 208, 1243–1252. <https://doi.org/10.1084/jem.20102477>.
 29. Victora, G.D., Schwickert, T.A., Fooksman, D.R., Kamphorst, A.O., Meyer-Hermann, M., Dustin, M.L., and Nussenzweig, M.C. (2010). Germinal center dynamics revealed by multiphoton microscopy with a photoactivatable fluorescent reporter. *Cell* 143, 592–605. <https://doi.org/10.1016/j.cell.2010.10.032>.
 30. Zaheen, A., Boulian, B., Parsa, J.Y., Ramachandran, S., Gommerman, J.L., and Martin, A. (2009). AID constrains germinal center size by rendering B cells susceptible to apoptosis. *Blood* 114, 547–554. <https://doi.org/10.1182/blood-2009-03-211763>.
 31. Inoue, T., and Kurosaki, T. (2024). Memory B cells. *Nat. Rev. Immunol.* 24, 5–17. <https://doi.org/10.1038/s41577-023-00897-3>.
 32. Zhang, Y., Meyer-Hermann, M., George, L.A., Figge, M.T., Khan, M., Goodall, M., Young, S.P., Reynolds, A., Falciani, F., Waisman, A., et al. (2013). Germinal center B cells govern their own fate via antibody feedback. *J. Exp. Med.* 210, 457–464. <https://doi.org/10.1084/jem.20120150>.
 33. Bonsignori, M., Zhou, T., Sheng, Z., Chen, L., Gao, F., Joyce, M.G., Ozorowski, G., Chuang, G.Y., Schramm, C.A., Wiehe, K., et al. (2016). Maturation Pathway from Germline to Broad HIV-1 Neutralizer of a CD4-Mimic Antibody. *Cell* 165, 449–463. <https://doi.org/10.1016/j.cell.2016.02.022>.
 34. Abbott, R.K., Lee, J.H., Menis, S., Skog, P., Rossi, M., Ota, T., Kulp, D.W., Bhullar, D., Kalyuzhnii, O., Havener-Daughton, C., et al. (2018). Precursor Frequency and Affinity Determine B Cell Competitive Fitness in Germinal Centers, Tested with Germline-Targeting HIV Vaccine Immunogens. *Immunity* 48, 133–146.e6. <https://doi.org/10.1016/j.jimmuni.2017.11.023>.
 35. Woodruff, M.C., Kim, E.H., Luo, W., and Pulendran, B. (2018). B Cell Competition for Restricted T Cell Help Suppresses Rare-Epitope Responses. *Cell Rep.* 25, 321–327.e3. <https://doi.org/10.1016/j.celrep.2018.09.029>.
 36. Yeh, C.H., Nojima, T., Kuraoka, M., and Kelsoe, G. (2018). Germinal center entry not selection of B cells is controlled by peptide-MHCII complex density. *Nat. Commun.* 9, 928. <https://doi.org/10.1038/s41467-018-03382-x>.
 37. Hua, Z., and Hou, B. (2020). The role of B cell antigen presentation in the initiation of CD4+ T cell response. *Immunol. Rev.* 296, 24–35. <https://doi.org/10.1111/imr.12859>.
 38. Purtha, W.E., Tedder, T.F., Johnson, S., Bhattacharya, D., and Diamond, M.S. (2011). Memory B cells, but not long-lived plasma cells, possess antigen specificities for viral escape mutants. *J. Exp. Med.* 208, 2599–2606. <https://doi.org/10.1084/jem.20110740>.
 39. Krebs, S.J., Kwon, Y.D., Schramm, C.A., Law, W.H., Donofrio, G., Zhou, K.H., Gifit, S., Dussupt, V., Georgiev, I.S., Schätzle, S., et al. (2019). Longitudinal Analysis Reveals Early Development of Three MPER-Directed Neutralizing Antibody Lineages from an HIV-1-Infected Individual. *Immunity* 50, 677–691.e13. <https://doi.org/10.1016/j.jimmuni.2019.02.008>.
 40. Bullard, B.L., and Weaver, E.A. (2021). Strategies Targeting Hemagglutinin as a Universal Influenza Vaccine. *Vaccines (Basel)* 9, 257. <https://doi.org/10.3390/vaccines9030257>.
 41. Goodnow, C.C., Crosbie, J., Adelstein, S., Lavoie, T.B., Smithgill, S.J., Brink, R.A., Pritchardbriscoe, H., Wotherspoon, J.S., Loblay, R.H., Raphael, K., et al. (1988). Altered Immunoglobulin Expression and Functional Silencing of Self-Reactive Lymphocytes-B in Transgenic Mice. *Nature* 334, 676–682. <https://doi.org/10.1038/334676a0>.

42. Tiller, T., Busse, C.E., and Wardemann, H. (2009). Cloning and expression of murine Ig genes from single B cells. *J. Immunol. Methods* 350, 183–193. <https://doi.org/10.1016/j.jim.2009.08.009>.
43. Scheres, S.H.W. (2012). A Bayesian View on Cryo-EM Structure Determination. *J. Mol. Biol.* 415, 406–418. <https://doi.org/10.1016/j.jmb.2011.11.010>.
44. Adams, P.D., Afonine, P.V., Bunkóczki, G., Chen, V.B., Davis, I.W., Echols, N., Headd, J.J., Hung, L.W., Kapral, G.J., Grosse-Kunstleve, R.W., et al. (2010). PHENIX: a comprehensive Python-based system for macromolecular structure solution. *Acta Crystallogr. D Biol. Crystallogr.* 66, 213–221. <https://doi.org/10.1107/S0907444909052925>.
45. Emsley, P., and Cowtan, K. (2004). Coot: model-building tools for molecular graphics. *Acta Crystallogr. D Biol. Crystallogr.* 60, 2126–2132. <https://doi.org/10.1107/S0907444904019158>.
46. Punjani, A., Rubinstein, J.L., Fleet, D.J., and Brubaker, M.A. (2017). cryo-SPARC: algorithms for rapid unsupervised cryo-EM structure determination. *Nat. Methods* 14, 290–296. <https://doi.org/10.1038/nmeth.4169>.
47. Hou, B., Reizis, B., and DeFranco, A.L. (2008). Toll-like receptors activate innate and adaptive immunity by using dendritic cell-intrinsic and -extrinsic mechanisms. *Immunity* 29, 272–282. <https://doi.org/10.1016/j.immuni.2008.05.016>.
48. Scheres, S.H.W. (2012). A Bayesian view on cryo-EM structure determination. *J. Mol. Biol.* 415, 406–418. <https://doi.org/10.1016/j.jmb.2011.11.010>.
49. Bao, K., Zhang, X., Li, D., Sun, W., Sun, Z., Wang, J., and Zhu, P. (2022). In situ structures of polymerase complex of mammalian reovirus illuminate RdRp activation and transcription regulation. *Proc. Natl. Acad. Sci. USA* 119, e2203054119. <https://doi.org/10.1073/pnas.2203054119>.
50. Zhu, D., Wang, X., Fang, Q., Van Etten, J.L., Rossmann, M.G., Rao, Z., and Zhang, X. (2018). Pushing the resolution limit by correcting the Ewald sphere effect in single-particle Cryo-EM reconstructions. *Nat. Commun.* 9, 1552. <https://doi.org/10.1038/s41467-018-04051-9>.

STAR★METHODS

KEY RESOURCES TABLE

REAGENT or RESOURCE	SOURCE	IDENTIFIER
Antibodies		
Anti-Mouse-CD45R/B220 PE-CF594(clone RA3-6B2)	BD Biosciences	Cat#562290; RRID: AB_11151901
Anti-Mouse-CD19 APC-Cy7(clone 1D3)	BD Biosciences	Cat#557655; RRID: AB_396770
Anti-Mouse-IgM PE-Cy7(clone II/41)	Invitrogen	Cat#25-5790-82; RRID: AB_469655
Anti-Mouse-IgD BV711 (clone 11-26c.2a)	BioLegend	Cat#405731; RRID: AB_2563342
Anti-Mouse-GL-7 PE (clone GL7)	BD Biosciences	Cat#561530; RRID: AB_10715834
Anti-Mouse-CD8a PerCP-Cy5.5 (clone 53–6.7)	Invitrogen	Cat#45–0081; RRID: AB_1107004
Anti-Mouse-CD38 Alexa Fluor 700 (clone 90)	Invitrogen	Cat#56-0381-82; RRID: AB_657740
Anti-Mouse-GL-7 FITC (clone GL7)	BioLegend	Cat#144603; RRID: AB_2561696
Anti-Mouse-CD45.1 Pacific Blue (clone A20)	BioLegend	Cat#110722; RRID: AB_492866
Anti-Mouse-CD45.1 FITC (clone A20)	Invitrogen	Cat#11-0453-82; RRID: AB_465058
Anti-Mouse-CD45.1 Alexa Fluor 700 (clone A20)	BioLegend	Cat#110724; RRID: AB_493732
Anti-Mouse-CD45.2 APC-eFluor 780 (clone 104)	Invitrogen	Cat#47-0454-82; RRID: AB_1272175
Anti-Mouse-IgMa PE (clone DS-1)	BD Biosciences	Cat#553517; RRID: AB_396542
Biotin Anti-Mouse-CD45.1 (Clone A20)	BD Biosciences	Cat#553774 RRID: AB_395042
Biotin Anti-Mouse-CD45.2 (clone 104)	BD Biosciences	Cat#553771 RRID: AB_395040
Biotin Anti-Mouse IgG1(clone A85-1)	BD Biosciences	Cat#553441; RRID: AB_394861
Biotin Anti-Mouse IgG2a [b] (clone 5.7)	BD Biosciences	Cat#553504; RRID: AB_394889
Biotin Anti-Mouse IgG2b (clone R12-3)	BD Biosciences	Cat#553393
Biotin Anti-Mouse IgG3 (clone R2-38)	BD Biosciences	Cat#553401; RRID: AB_394841
Biotin Anti-Mouse IgA (clone C10-1)	BD Biosciences	Cat#556978; RRID: AB_396543
Biotin Anti-Mouse IgD (clone 11-26c)	Invitrogen	Cat#13-5993-82; RRID: AB_466860
HRP-conjugated streptavidin	Jackson Immunoresearch	Cat#016-030-084; RRID: AB_2337238
Anti-Human IgG1 Fc PE (HP6001)	SouthernBiotech	Cat#9054-09; RRID: AB_2796628
Goat anti-Mouse IgM-HRP	SouthernBiotech	Cat#1021-05; RRID: AB_2794240
Goat anti-Mouse IgG-Fc Fragment Antibody HRP Conjugated	Bethyl Laboratories	Cat# A90-131P; RRID: AB_67175
Anti-Human IgG (H + L) HPR Conjugate	Promega	Cat# W4031; RRID: AB_430835

(Continued on next page)

Continued

REAGENT or RESOURCE	SOURCE	IDENTIFIER
Bacterial and virus strains		
E. coli DH5a	Tsingke	Cat# TSC-C14
E. coli XL1-Blue	Tsingke	Cat# TSC-C14
Chemicals, peptides, and recombinant proteins		
Polyethylenimine (PEI)	Polyscience	Cat#23966-1
3,3'-Diaminobenzidine tetrahydrochloride hydrate	Sigma-Aldrich	Cat# D5637-1G
3,3',5,5'-Tetramethylbenzidine	Sigma-Aldrich	Cat#860336-1G
Fast Red	Sigma-Aldrich	Cat# F8764-1G
Recombinant Q β -AF647	Liao et al. ¹⁸	N/A
BV650 streptavidin	BioLegend	Cat#405231
Critical commercial assays		
Alexa Fluor 647 Protein Labeling Kit	Invitrogen	Cat# A20173
pClone007 Versatile Simple Vector Kit	Tsingke	Cat# TSV-007VS
Frist-Strand cDNA Synthesis SuperMix	TransGen Biotech	Cat# AT301
Protein A Sefinose	BBI Life Science	Cat# C600951
Immobilized Papain	Thermo	Cat# 20341
AHC Biosensors	Octet	Cat# 18-5060
Proteina Biosensors	Octet	Cat# 18-5010
Streptavidin (SA) Biosensors	Octet	Cat# 18-5019
CM5 Biosensors	Cytiva	Cat# 29104988
Deposited data		
Cryo-EM structure of Q β -Ab1	This paper	PDB: 8W5D; EMD-37286
Cryo-EM structure of Q β -Ab4	This paper	PDB: 8W5E; EMD-37287
Cryo-EM structure of Q β -Ab6	This paper	PDB: 8W5F; EMD-37290
Cryo-EM structure of Q β -Ab7	This paper	PDB: 8W5G; EMD-37291
Cryo-EM structure of Q β -Ab8	This paper	PDB: 8W5W; EMD-37306
Cryo-EM structure of Q β -Ab10	This paper	PDB: 8W5H; EMD-37292
Cryo-EM structure of Q β -Ab14	This paper	PDB: 8W5I; EMD-37293
Cryo-EM structure of Q β -Ab16	This paper	PDB: 8W5L; EMD-37296
Cryo-EM structure of Q β -Ab17	This paper	PDB: 8W5M; EMD-37297
Cryo-EM structure of Q β -Ab21	This paper	PDB: 8W5N; EMD-37298
Cryo-EM structure of Q β -Ab31	This paper	PDB: 8W5O; EMD-37299
Cryo-EM structure of Q β -Ab40	This paper	PDB: 8W5P; EMD-37300
Cryo-EM structure of Q β -Ab45	This paper	PDB: 8W5Q; EMD-37301
Cryo-EM structure of Q β -Ab53	This paper	PDB: 8W5R; EMD-37302
Cryo-EM structure of Q β -Ab57	This paper	PDB: 8W5T; EMD-37303
Cryo-EM structure of Q β ^{N10F} -Ab40	This paper	PDB: 8W5U; EMD-37304
Cryo-EM structure of Q β ^{N10K} -Ab40	This paper	PDB: 8W5V; EMD-37305
Experimental models: Cell lines		
Expi293F cells	Gibco	Cat# A14635
ExpiCHO cells	Cell Bank of the Chinese Academy of Sciences, Shanghai, China	Cat#12200036
Experimental models: Organisms/strains		
C57BL/6	The institute of Biophysics, Chinese Academy of Sciences	N/A
BoyJ	Jackson Laboratory	Cat#002014; RRID: IMSR_JAX:002014
Rag1 ^{-/-}	Jackson Laboratory	Cat#034159; RRID: IMSR_JAX:034159
Aicda ^{-/-}	The institute of Biophysics, Chinese Academy of Sciences	N/A

(Continued on next page)

Continued

REAGENT or RESOURCE	SOURCE	IDENTIFIER
MD4	Goodnow et al. ⁴¹	N/A
Oligonucleotides		
Primers for VH and V κ antibody heavy and light chain sequence reverse-transcription and nested PCR	Tiller et al. ⁴²	N/A
Recombinant DNA		
pET21-Q β -variant, G9A, G9S, G9F, G9K, N10A, N10F, N10K, N10A.T7A, N10A.D14A, N10A.K16A, N10A.T7A.D14A	This paper	N/A
Software and algorithms		
FlowJo 10.7.1	BD	https://www.flowjo.com/
IMGT/V-QUEST	N/A	https://www.imgt.org/IMGT_vquest/analysis
Biacore T100 evaluation software	GE Healthcare	https://www.cytilifesciences.com/en/us/support/software
Octet Data Analysis HT software	Fortebio	https://www.sartorius.com/en/products/protein-analysis/octet-systems-software
Graph Pad Prism version 10.0.2	GraphPad	https://www.graphpad.com
Adobe Illustrator 2023	Adobe	https://www.adobe.com/products/illustrator/
RELION	Scheres et al. ⁴³	https://www2.mrc-lmb.cam.ac.uk/relion
UCSF Chimera	N/A	https://www.cgl.ucsf.edu/chimera/
UCSF ChimeraX	N/A	https://www.rbvi.ucsf.edu/chimerax/
PHENIX	Adams et al. ⁴⁴	https://www.phenix-online.org
Coot	Emsley et al. ⁴⁵	https://www2.mrc-lmb.cam.ac.uk/Personal/pemsley/coot
cryoSPARC	Punjani et al. ⁴⁶	https://cryosparc.com
Pymol	N/A	https://pymol.org/

EXPERIMENTAL MODEL AND STUDY PARTICIPANT DETAILS

Experimental animals

All mice used in this study were housed under specific pathogen-free conditions, and their use was approved by the Animal Care and Use Committee of the Institute of Biophysics, Chinese Academy of Sciences. C57BL/6 mice (CD45.2) were either bred in-house or purchased from SPF Biotechnology Co., Ltd (China). CD45.1 BoyJ mice (JAX 002014) and *Rag1*^{−/−} mice were originally obtained from the Jackson Laboratory. MD4 mice were originally from Goodnow lab.⁴¹ *Aicda*^{−/−} mice used in this study were generated using CRISPR/Cas9 gene knockout technology and were back-crossed to C57BL/6 mice for at least six generations. Mixed bone marrow chimeric mice were generated by transplanting a mixture of BoyJ and C57BL/6 (at a 1:1 ratio) or BoyJ and *Aicda*^{−/−} (at a 1:1 ratio) mouse bone marrow cells into lethally irradiated (1000 rad) C57BL/6 mice.

Cell lines and culture conditions

Expi293F cells (Gibco, USA) were cultured in SMM 293-TII medium (Sino Biological Inc, China) as suspension cultures at 37°C with 5% CO₂, with shaking at 125 rpm/min. CHO cells (12200036, Cell Bank of the Chinese Academy of Sciences, Shanghai, China) were propagated in IMDM medium (HyClone, Logan, UT, USA) supplemented with 10% fetal bovine serum (Biological Industries, IL). The cells were maintained at 37°C in a 5% CO₂ incubator, and subcultures were performed every 2–3 days.

METHOD DETAILS

Expression and purification of Q β -VLP and variants

To obtain variants, single or multiple point mutations were introduced into the high-frequency binding amino acids on the Q β -VLP sequence using PCR. The expression and purification of Q β -VLP and its variant forms were performed as previously described.¹⁸

Immunization

Littermates of the same sex, aged 8–12 weeks or 8 weeks post-transplantation, were randomly assigned to experimental groups. Male and female mice were intraperitoneally injected with 25 µg of purified Q β -VLPs in 200 mL of PBS.

Adoptive transfer

No Q β -AF647 (mock-depleted) or 1 µg of Q β -AF647 (depleted) was added to 200 µL of splenocytes suspension, with a final Q β -AF647 concentration ~2 nM. The cells were placed at 4°C in the dark for 30 min and then washed with FACS buffer. Cells were then incubated with 15 µL anti-Cy5/AF647 MicroBeads and passed through a magnetic column (both from Miltenyi Biotec). 2 × 10⁷ cells from the flow-through fraction were transferred to recipient mice by tail-vein injection 1 day before immunization. Depleted and mock-depleted lymphocytes were isolated from spleens of C57BL/6 (CD45.2 $^{+}$) and BoyJ (CD45.1 $^{+}$) mice alternately and used for transfer to minimize potential bias.

Most adoptive transfer experiments were performed using *Rag1*^{−/−} mice as recipients. To determine whether the structural aberrations in the spleens of *Rag1*^{−/−} mice might influence the outcome of GC competition, MD4 mice were used as recipients for the mixed transfer experiment. No significant differences were observed in Q β $^{+}$ GC B cells derived from the Q β -depleted or mock-depleted fractions when MD4 mice were used as recipients (Figures S2C–S2E).

A routine dose of 25 µg of Q β -VLP was used for immunization in the adoptive transfer experiments. When a lower dose (1 µg) of Q β -VLP was administered, significantly fewer Q β $^{+}$ GC B cells were generated from the transferred cells. Moreover, the GC B cells derived from the mock-depleted fractions were significantly more abundant than those from the Q β -depleted fractions (Figures S2F–S2I). This result suggested that an optimal GC response is necessary for low-affinity B cells to succeed in the competition. The effect of antigen dose on the GC competition was not further investigated in this study.

Labeling and enrichment of antigen-specific B cells

The labeling and enrichment of Q β -specific B cells were conducted following previously described methods.¹⁸ In brief, labeling kits (Thermo Fisher Scientific) were used to conjugate AF647 to lysine residues on Q β -VLP at a sparse ratio (12–16%) to minimize antigen perturbation. Enzymatically dissociated splenocytes were treated with Q β -AF647 at a concentration of 2 nM and incubated at 4°C for 30 min. Subsequently, the cells were incubated with anti-AF647 microbeads (Miltenyi Biotec) and isolated using a magnetic column (Miltenyi Biotec). In cases where distinction between Q β $^{+}$ and AF647 $^{+}$ B cells was required, Q β -GFP was added at a concentration of 2 nM.

Flow cytometry

Mouse spleen was digested with collagenase II and DNase I (both from Worthington) in RPMI 1640 (Invitrogen) with 25 mM HEPES (pH 7.5). The splenocytes were then washed in FACS buffer (2% newborn calf serum, 2 mM EDTA, and 0.1% NaN₃ in PBS) and blocked with anti-CD16/32 mAb. Flow cytometry analysis utilized the following antibodies and reagents: FITC anti-CD45.1 (30-F11), AF700 anti-CD45.1 (A20), Pacific Blue anti-CD45.1 (A20), allophycocyanin-Cy7 anti-CD45.2 (104), PE-CF594 anti-B220 (RA3-6B2), allophycocyanin-Cy7 anti-CD19 (1D3), PE-Cy7 anti-IgM (II/41), BV711 anti-IgD (11-26c.2a), PE anti-GL-7 (GL7), AF700 anti-CD38 (90), PerCP-Cy5.5 anti-CD8 (53–6.7), and PE anti-human IgG1-Fc (9054-09). Data acquisition was performed using an LSR II cytometer (Becton Dickinson, USA) and analyzed using FlowJo software (TreeStar, USA).

Single cell sorting and cDNA synthesis

Q β $^{+}$ GC B cells were sorted from the Q β -AF647-enriched cell fractions as Q β -AF647 $^{+}$ B220 $^{+}$ CD19 $^{+}$ CD38 $^{-}$ GL-7 $^{+}$ cells. Sorting was performed using a BD FACS Aria III into DEPC-treated PBS containing 2% FBS, achieving purities of 95–98%.

After sorting, single cells were manually selected under a microscope using micropipettes and transferred into the reverse transcription (RT) system for cell lysis and RT. RT reactions were performed using constant region primers, as previously described,⁴² at 25°C for 10 min, 42°C for 30 min, and 85°C for 5 min. The synthesized cDNA was stored at –30°C.

Ig gene amplification

The variable region of Ig gene was amplified following previously described protocol.⁴² For IgH and Igκ V gene transcripts, independent nested PCR amplification was performed using 4 µL of cDNA as a template. Each PCR reaction was carried out in a total volume of 25 µL per well, containing a primer mix at a concentration of 40 nM (primers sequence were chosen same as previous publications and the concentration modified based on Tiller et al., 2009), 300 nM of each dNTP (TransGen Biotech Co.), and 1.2 U of Taq DNA polymerase (Biomed). All primers were stored in small aliquots to avoid repeated freezing and thawing, and all PCRs were performed using nuclease-free water. The nested second round PCR reactions with gene-specific primers or primer mixes utilized 2.2 µL of the unpurified first PCR product.

The first round of PCR consisted of 50 cycles with the following conditions: 94°C for 30 s, 56°C (IgH) or 50°C (Igκ) for 30 s, and 72°C for 55 s. The second round of PCR consisted of 50 cycles with the following conditions: 94°C for 30 s, 60°C (IgH) or 45°C (Igκ) for 30 s, and 72°C for 45 s. The PCR products were subsequently cloned into a T-vector, and clones from each transformation were subjected to Sanger sequencing. Nucleotide sequences were analyzed using IMGT/V-Quest (<http://www.imgt.org>) to identify germline V, D, and J gene members with the highest sequence homology.

The overall success rate for amplifying both IgH and Igκ genes from single cells was approximately 50%. Over 100 paired sequences were obtained in this study, and more than 90% of them were successfully expressed in recombinant form. The origin and sequence information for each antibody are provided in [Table S1](#). Clones with repeated usage of VH, Vκ, and CDR3 regions are indicated in the table.

Expression and purification of antibodies and Fab fragments

The Ig sequences were cloned directly into expression vectors containing the human IgG1 and Igκ constant regions, following previously described methods.⁴² Antibodies were expressed by transient co-transfection of heavy and light chain plasmids using PEI into Expi293F cells in suspension cultures, incubated at 37°C for 4–5 days. The cell supernatants were then passed over Protein A agarose (BBI Life Sciences) for purification.

Fab fragments were generated by digesting the IgG using Immobilized Papain (Thermo). The resulting Fab and Fc mixture was subsequently passed back over Protein A agarose to remove Fc fragments. The yield of the Fab fragments was assessed by measurement using nanodrop and PAGE analysis. The purified proteins were exchanged into PBS as buffer and stored at –80°C.

Enzyme-linked immunosorbent assay (ELISA)

The ELISA procedure was conducted following the previously described methods.⁴⁷ In summary, serially diluted sera were incubated with antigen-coated plates. Horseradish peroxidase (HRP)-conjugated anti-mouse IgG (Bethyl Laboratories), anti-mouse IgM (Southern Biotech), or anti-human IgG1-Fc (Promega) antibodies were used for detection. The HRP substrate used was 3,3',5,5'-tetramethylbenzidine (Sigma-Aldrich). Optical density measurements were obtained at 450 nm and 570 nm using a microplate reader (SpectraMax, Molecular Devices). The anti-Qβ titers in mouse sera were determined as the reciprocal of the highest dilution resulting in an optical density value (450–570 nm) exceeding ten times the standard deviation value measured from the serum-free wells.

To evaluate the resistance of Qβ-specific monoclonal antibodies to antigen mutations, plates were coated with Qβ-VLP or its mutated variants. Each tested antibody was subjected to a 5-fold dilution gradient starting at 200 μg/mL. The binding capabilities of the antibodies to Qβ^{WT} or its variants were quantified and compared using the area under the curve (AUC). Antibodies exhibiting a reduction in AUC of more than 10% when binding to the variant Qβ-VLP compared to the binding to the Qβ^{WT} were considered non-cross-reactive.

Measurement of binding kinetics by surface plasmon resonance (SPR)

SPR was conducted using a BIACore T100 instrument. The determination of apparent affinities involved capturing approximately 500 RU of Qβ-VLP on a CM5 sensor chip (GE Healthcare) surface using the NHS/EDC method. A PBS running buffer supplemented with 0.05% Tween 20 was prepared for the assay. Serial dilutions of Fabs were flowed over the immobilized Qβ-VLP, with each concentration of Fabs being flowed over for 60 s at a rate of 30 μL/min. The dissociation phase was measured for 60–360 s. To regenerate the surface between injections, glycine pH 1.7 was injected for 30 s. The binding kinetics, K_{on} ($M^{-1}s^{-1}$), K_{off} (s^{-1}), and K_D (M) were calculated from global fittings using a 1:1 kinetics binding model on the Biacore T100 evaluation software (GE Healthcare).

Measurement of binding kinetics by biolayer interferometry (BLI)

BLI experiments were conducted using an Octet Red 96 instrument (ForteBio). AHC biosensors (ForteBio) were used to immobilize monoclonal anti-Qβ antibodies. Qβ-VLP in PBS with 2-fold serial dilutions served as analytes, with incubation time of 120 s, followed by a dissociation phase of 360 s. The experimental data was analyzed using the Octet BLI Analysis 9.1 software (ForteBio) employing a 1:1 fitted model.

Competitive inhibition assay

To estimate the affinity of membrane-bound antibodies in GC B cells isolated from mice or CHO cells expressing recombinant antibodies, a competitive inhibition assay was performed as previously described.¹⁸ Pooled cells were divided equally into eight fractions. Serially diluted unlabeled Qβ-VLPs were added to each fraction and incubated on ice for 30 min. Subsequently, Qβ-AF647 was added to the cells at a concentration of 0.2 nM, without removing the unlabeled Qβ-VLPs. Flow cytometry was performed to detect Qβ-AF647⁺ cells. The number of Qβ-AF647⁺ cells in each fraction was normalized to the fraction without the presence of unlabeled Qβ-VLPs. The obtained data were analyzed by fitting curves using Prism software, employing the three-parameter log-response model. The resulting half-maximal inhibitory concentrations (IC_{50}) value, representing the concentration of unlabeled Qβ-VLP required to inhibit 50% of Qβ-AF647 binding, was used as an indicator of the antibody's affinity.

In the modified competitive inhibition assay, splenocytes were incubated with a fixed concentration of unlabeled Qβ-VLP, followed by binding to Qβ-AF647. The number of Qβ⁺ cells in the presence or absence of unlabeled Qβ-VLP (designated as $Q\beta^+cell_{block}$ and $Q\beta^+cell_{unblock}$) was used to calculate the blocking ratio, which was determined as $1 - (Q\beta^+cell_{block}/Q\beta^+cell_{unblock})$. The concentration of unlabeled Qβ-VLP was set to ~0.6 nM for samples collected at day 7 post-immunization and ~0.06 nM for samples collected at day 14 post-immunization.

Negative staining electron microscopy analysis

To assess the structural integrity of Q β -VLP variants using electron microscopy (EM), 5 μ L of purified Q β -VLP variants were applied to glow-discharged, carbon-coated grids and stained with 1% phosphotungstic acid (pH 7.0). The grids were transferred to an FEI Tecnai 20 transmission electron microscope for visualization.

Cryo-EM data collection, processing and structure building

Antibodies cloned from the indicated sources were confirmed to bind Q β -VLP before being randomly selected for structural studies, with consideration given to maximize the coverage of different VH/Vk usages.

The purified Q β -VLP and the variants were incubated with Fabs on ice for 30 min. Then, aliquots of 3.5 μ L of Q β -VLP-Fab complex were applied to newly glow-discharged holy Ni-Ti film grids (R1.2/1.3, 300 meshes, Au, Zhenjiang Lehua Electronic Technology Co., LTD, China). The grids were blotted for 2.5 s in a 100% humidity chamber and plunged into liquid ethane (cooled by liquid nitrogen) in an FEI Vitrobot Mark IV vitrification robot (Thermo Fisher Scientific, USA).

For some Q β -VLP-Fab complexes, dose-fractionated super-resolution movies were collected using a 300-kV FEI Titan Krios electron microscope or a 200-kV FEI Arctica electron microscope (Thermo Fisher Scientific, USA) with a K2 direct electron detector (Gatan Company, USA). For some Q β -VLP-Fab complexes aiming at epitope mapping, micrographs were collected using a 200-kV FEI Talos F200C electron microscope or a 120-kV FEI Talos L120C electron microscope (Thermo Fisher Scientific, USA) with a Ceta camera (Thermo Fisher Scientific, USA). Data processing was carried out using cryoSPARC⁴⁶ and Relion.⁴⁸ After 2D classification, “good” particles were selected for 3D reconstruction applying icosahedral symmetry. To improve the density surrounding Fabs possessing two epitopes on Q β dimer with steric clash, we performed block-based asymmetric reconstruction.^{49,50} Briefly, sub-particles around the Fabs were extracted according to their locations and orientations obtained by icosahedral reconstruction. No-alignment 3D classifications and local reconstructions were carried out using Relion and cryoSPARC. Structural modeling and refinement were performed using Coot⁴⁵ and Phenix.⁴⁴ Detailed structure information is listed in [Table S2](#).

QUANTIFICATION AND STATISTICAL ANALYSIS

Statistical analysis

Statistical analysis was performed with GraphPad Prism, with p -values <0.05 considered statistically significant.